An Abstract of the Thesis of

David Alan Pimentel for the degree of Master of Science in Nuclear Engineering and Mechanical Engineering presented on May 9, 1996.

Title: Two-Phase Fluid Break Flow Measurements and Scaling in the Advanced Plant Experiment (APEX).

Abstract approved:

José N. Reyes

Lorin R. Davis

The Oregon State University (OSU) Advanced Plant Experiment (APEX) is a one-fourth height, one-half time scale, reduced pressure integral systems test facility designed to model the long-term cooling capabilities of the emergency core cooling systems of the Westinghouse AP600. This study provides a brief description of the APEX test facility, analyzes the measured flow rates through the simulated break geometry, and compares the data with existing flow models.

The break flow rates of various tests have been measured using state-of-the-art instrumentation: magnetic meters for liquid flows and vortex meters for vapor flows. The flow rate data has been reported with corresponding instrument measurement errors. In addition to the flow meters 'measurements, the liquid-level-depression-rate within the pressurizer was determined for simulated break sizes of one inch or less. Based upon a simple mass balance, the initial break flow rates were calculated using the pressurizer draining rates, and the calculated values were found to be in good agreement with that of the flow meters. The following flow models were also used to predict the initial break flow rates: Homogeneous Equilibrium Model, Equilibrium Rate Model, and Henry-Fauske Subcooled Model. The Henry-Fauske Subcooled Model yielded the most accurate flow predictions when saturated conditions were assumed at a given system pressure.

The break flow measurements were also compared to a simple integrated mass model which assumes a constant mass flow rate due to choked flow conditions. This correlation yielded results in

good agreement with the total mass loss through the break. The results were presented in a non-dimensional form.

Two-Phase Fluid Break Flow Measurements and Scaling in the Advanced Plant Experiment (APEX)

by

David Alan Pimentel

A THESIS

submitted to
Oregon State University

in partial fulfillment of
the requirements for the
degree of

Master of Science

Completed May 9, 1996
Commencement June, 1996

Master of Science thesis of David Alan Pimentel presented on May 9, 1996.

APPROVED:

Co-Major Professor, representing Nuclear Engineering

Co-Major Professor, representing Mechanical Engineering

Head of Department of Nuclear Engineering

Head of Department of Mechanical Engineering

Dean of Graduate School

I understand that my thesis will become part of the permanent collection of Oregon State University libraries. My signature below authorizes release of my thesis to any reader upon request.

David Alan Pimentel, Author

Acknowledgments

I ð like to thank Dr. José N. Reyes for allowing me the opportunity to draw knowledge and advice from him over the past six years as both an undergraduate and a graduate student.

Table of Contents

Page

Table of Contents (Continued)

Page

List of Figures

List of Figures (Continued)

List of Tables

Nomenclature

General Symbols

A	cross-sectional flow area (m^2)
C_D	nozzle discharge coefficient
c_p	specific heat capacity (J/kg^oK)
D	diameter (m)
G	mass flow rate per unit area (kg/m^2s)
g	gravitational acceleration (9.80665 m/s^2)
h	enthalpy (J/kg)
K	flow resistance coefficient
L	fluid level (m)
L/D	length-to-diameter ratio for a duct
l_w	actual duct length (m)
M	mass (kg)
M^*	fraction of mass remaining above the break elevation $\left(\frac{M_0 - M_e}{M_0}\right)$
M'	M^* normalized to time of ADS-1 actuation
$\dot{m}$	mass flow rate (kg/s)
N	non equilibrium flow parameter in Relaxation Length Model
N_s	experimental parameter in Henry-Fauske Subcooled Flow Model
P	pressure (Pa)
s	entropy (J/kg^oK)
T	temperature (^oK)
t	time (seconds)
V	velocity (m/s)
v	specific volume (m^3/kg)
$\forall$	volume (m^3)
x	vapor mass fraction (quality)
z	axial direction (m)

Greek Symbols

a	vapor void fraction
Δ	denotes a differential value (i.e., $\Delta P = P - P'$)
g	specific heat ratio $\left(\frac{c_p}{c_v}\right)$
l	critical duct length required for the development of equilibrium flow determined by Fauske (0.10 m)
m	dynamic viscosity (kg/ms)
f	modeled dimensionless group $\left(1 - w_0 t\right)$

f'	f normalized to time of ADS-1 actuation
r	fluid density (kg/m^3)
w	specific frequency of continuum (s^{-1})

Subscripts

0	initial condition (time equals zero)
$ADS-1$	time of ADS-1 actuation
$Break$	condition at the break location
c	critical (choked) flow condition
E	velocity, temperature and free-energy equilibrium for all phases
e	exit condition (i.e., break)
ERM	Equilibrium Rate Model
f	saturated liquid property
fg	saturated vapor property value - saturated liquid property value
g	saturated vapor property
HEM	Homogeneous Equilibrium Model
k	arbitrary fluid phase
m	fluid mixture property
o	stagnation condition
OEM	Orifice Equation Model
p	evaluated at a constant pressure
r	receiver condition
pzr	pressurizer condition
RLM	Relaxation Length Model
S	evaluated at a constant entropy
sat	saturation condition
sys	system property or condition
T	evaluated at a constant temperature
t	nozzle-throat condition
TP	two-phase fluid mixture
V	evaluated at a constant volume

Dedication

This document is dedicated to my wife, Donna, who sacrificed her immediate desires by allowing me the time I needed to complete it. I thank God for her patience and support.

Two-Phase Fluid Break Flow Measurements and Scaling in the Advanced Plant Experiment (APEX)

1. Introduction

The quantification of mass lost through a pressurized system rupture is important to full understanding of the depressurization behavior of a wide variety of boiler systems. Of particular interest is the effect of system depressurization on the integrated safety systems of Westinghouse's next generation nuclear power plant, the AP600. The Oregon State University (OSU) Advanced Plant Experiment (APEX) test facility is designed to model the AP600 small break loss of coolant accidents '(LOCA) long-term cooling behaviors. An important aspect of the test matrix is the quantification of primary mass inventory losses through simulated system ruptures. This thesis describes the methods used to analyze the break flow measurements obtained in the OSU APEX test facility, and the objectives of this study include the following:

- Evaluate the instrumentation to accurately measure the initially-subcooled break flow rates and time-dependent saturated break flow rates for various test configurations.
- Compare the initial break flow rates with the predictions of several well-known critical flow models.
- Compare the time-dependent integrated mass exiting the break measured by the BAMS with the predictions of an integrated mass model.
- Present the results in terms of non-dimensional quantities.

Chapter two presents a brief review of two-phase fluid critical flow models. Chapter three presents a description of the APEX test facility. Chapter four presents an evaluation of the APEX break flow measurement system during subcooled depressurization. Chapter five presents an integrated mass method for collapsing the measured critical flow data onto a single dimensionless plot, and chapter six presents the conclusions of this research.

2. Review of Two-phase Critical Flow Models

For high pressure systems, it is reasonable to assume that critical flow conditions exist at the rupture. The critical flow rate through the rupture can be predicted given the initial stagnation properties of the system, and, under certain condition, the subsequent pressure history can be predicted using this initial flow rate.

Critical flow is defined by the following differential equation [1]:

$$\frac{dG}{dP} = 0, \tag{2-1}$$

and it corresponds to the maximum flow rate that can be achieved by a compressible fluid as it passes from a high-pressure region to a low pressure region. In many cases, a rupture's flow behavior is modeled as a nozzle. Figure 2-1 shows a two-dimensional view of such a nozzle and its corresponding pressure behavior with respect to position. Any further reduction of the exit pressure below the critical pressure, $P_{e,2}$, does not increase the flow rate through the nozzle. The maximum mass flux defined by Equation 2-1 corresponds to the throat of the nozzle, where the critical pressure ratio, $\frac{P_c}{P_o}$, exists.

As an example, the isentropic single phase mass efflux, based upon ideal gas relations, from a ruptured system is derived as

$$G = r_o \sqrt{2c_p T_o \left(1 - \frac{T}{T_o}\right)\left(\frac{P}{P_o}\right)^{2/g}}, \tag{2-2}$$

where the subscript, o, refers to stagnation properties of the fluid that correspond to a zero-velocity flow condition within the bulk fluid of the pressurized vessel [2]. Unfortunately, the analysis for two-phase flows cannot use the ideal gas relations. Thus, other methods of analysis must be used to predict choked flow. In the past, many attempts to predict this flow condition have proved it to be an overwhelming task. Included below are some brief descriptions of the more widely used and recent two-phase flow models available.

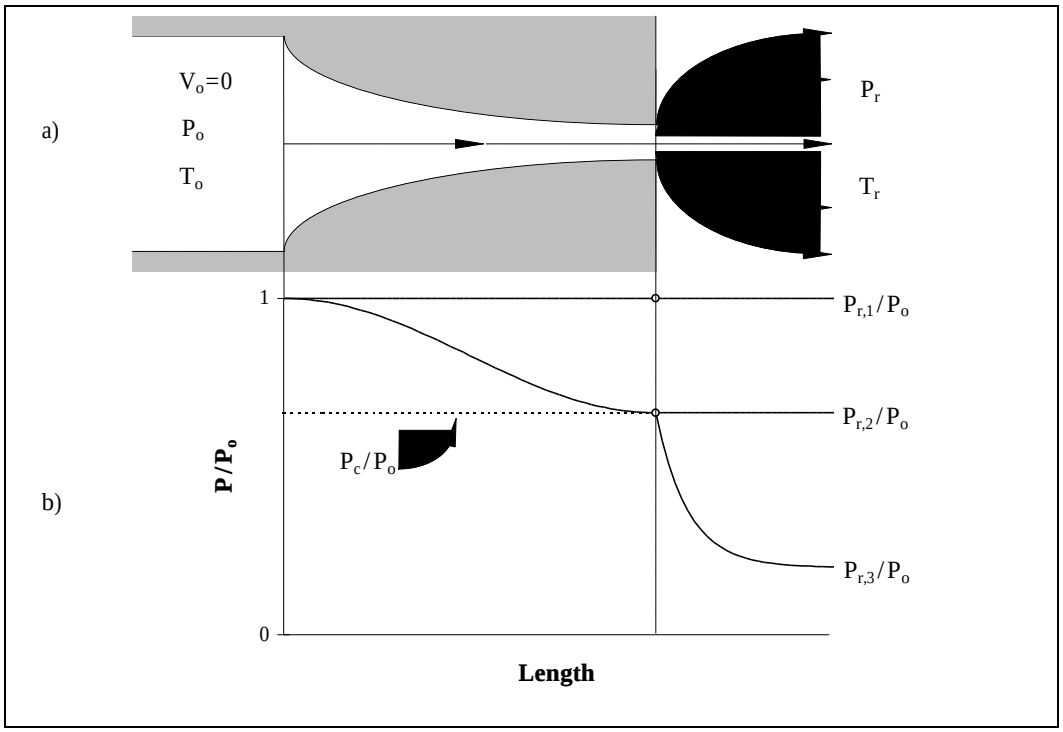

Figure 2-1. a) Generic converging nozzle diagram for the visualization of critical flow conditions. b) Typical variation in pressure as a function of position in a converging nozzle and of receiver pressure [1].

2.1 Homogeneous Equilibrium Model

One of the most widely used critical flow models is the Homogeneous Equilibrium Model (HEM) [2]. This is primarily due to its simplicity. The HEM assumes there exists no difference between the liquid and vapor velocities within a continuum. Also, the two-phases are assumed to exist at the same temperature and pressure. This flow model is derived from the relationship between the mixture mass flux, density and velocity,

$$G = r\,V\,. \tag{2-3}$$

From the first law of thermodynamics, the stagnation enthalpy is shown to be related to the critical (see Equation 2-1) enthalpy and velocity by

$$h_o = h + \frac{V^2}{2}\,. \tag{2-4}$$

Note this is a simple potential and kinetic energy balance for the fluid mixture. By assuming an isentropic expansion from the stagnation conditions to those at the critical point,

$$s = s_o, \tag{2-5}$$

and by assuming saturated stagnation and critical conditions, a critical mixture quality is determined to be

$$x = \frac{s - s_f}{s_{fg}}. \tag{2-6}$$

The saturated values, s_f and s_{fg}, are determined at the critical pressure, and s is determined as the saturated liquid entropy, s_f, at the stagnation pressure. Now, the expression for the mixture velocity, V, is determined from Equation 2-4 to be

$$V = \sqrt{2(h_o - h)}, \tag{2-7}$$

and the enthalpy, h, is calculated, using the saturated enthalpy values at the critical pressure, to be

$$h = h_f + x\left(h_g - h_f\right). \tag{2-8}$$

Similarly, the mixture density can be determined at the critical pressure in terms of the liquid and vapor specific volumes,

$$r = \{v_f + x(v_g - v_f)\}^{-1}. \tag{2-9}$$

Finally, incorporating Equations 2-7 through 2-9 into Equation 2-3 yields the following expression for the critical mass flux:

$$G_{HEM} = \frac{\sqrt{2(h_o - h_f - xh_{fg})}}{(v_f + xv_{fg})}. \tag{2-10}$$

Figure 2-2 shows the typical dependence of mass flux as a function of the pressure ratio. By varying the local pressure, Equations 2-3, 2-4, 2-8, and 2-9 yield the curve shown for a chosen critical vapor quality. The critical flow condition occurs at the critical pressure ratio as shown. The HEM has been shown to be a good approximation for critical flow at high flow rates and high stagnation pressures in pipe lengths greater than 30 cm [2].

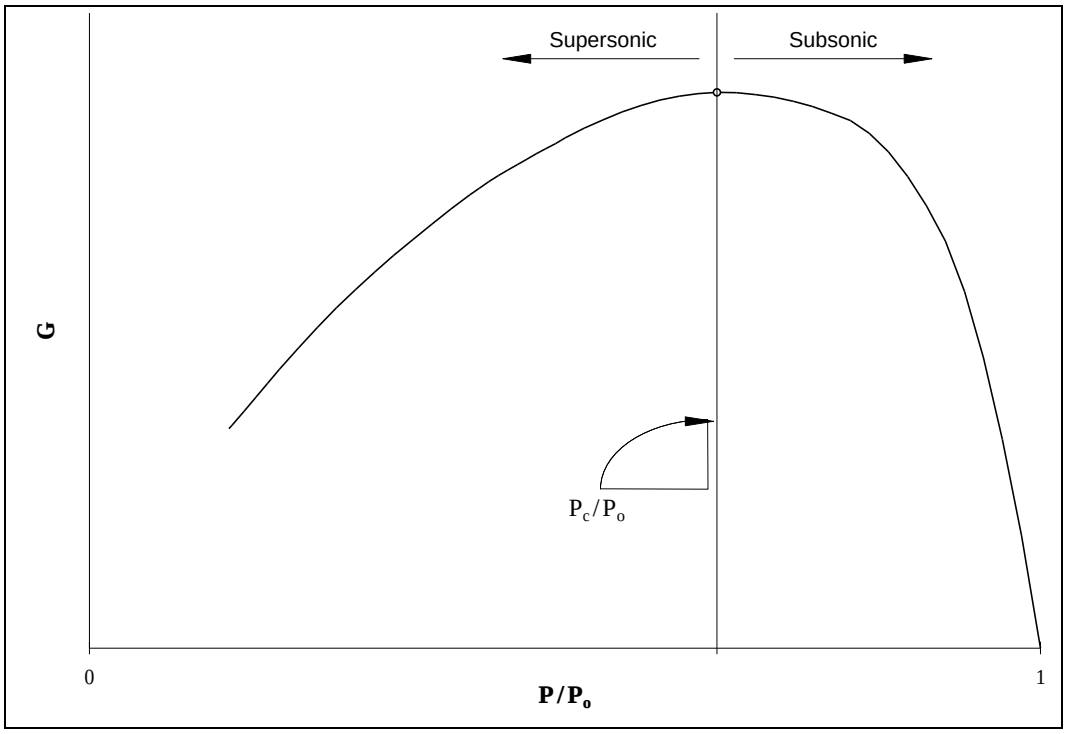

Figure 2-2. Typical variation in mass flow rate per unit area as a function of pressure ratio [3].

2.2 Equilibrium Rate Model

A superficial mass flux is defined as the phase-specific flow rate per unit cross-sectional flow area, or, for phase "k",

$$G_k \equiv \rho_k V_k \alpha_k \tag{2-11}$$

where ρ_k, V_k and α_k are the area-averaged magnitudes of density, velocity and void fraction respectively. For a vapor-liquid mixture, the total mass flux is

$$G_m \equiv \frac{1}{A}\frac{dM}{dt} = G_g + G_f \tag{2-12}$$

or

$$G_m = \rho_g V_g \alpha_g + \rho_f V_f \alpha_f . \tag{2-13}$$

If the liquid void fraction is stated in terms of the vapor void fraction,

$$\alpha_f = 1 - \alpha_g = 1 - \alpha \tag{2-14}$$

and a homogeneous mixture is assumed (i.e., $V_f = V_g = V_m$), the mixture mass flux becomes that of Equation 2-3,

$$G_m = \rho_f V_f (1-\alpha) + \rho_g V_g \alpha = \rho_m V_m . \tag{2-15}$$

For a critical mass flow rate, $\left(\frac{dM}{dt}\right)_c$, through a constant cross-sectional area, A, the following relation can be obtained from Equation 2-15:

$$\frac{d}{dP}\left(\frac{dM}{dt}\right)_c = \frac{\partial \rho_m}{\partial P} V_m A + \frac{\partial V_m}{\partial P} \rho_m A = 0 . \tag{2-16}$$

Rearranging Equation 2-16 yields

$$\left(\frac{\partial V_m}{\partial P}\right)_c = -\frac{V_m}{\rho_m}\frac{\partial \rho_m}{\partial P} \tag{2-17}$$

where the subscript, c, refers to critical flow conditions. The single-dimension momentum equation in the "z" direction for a Newtonian, incompressible fluid is

$$\frac{1}{A}\frac{dM}{dt}\frac{\partial V_z}{\partial z} = -\frac{\partial P}{\partial z} + \rho_m g_z + \mu \nabla^2 V_z . \tag{2-18}$$

By neglecting viscous and gravitational effects and by assuming a uniform flow mixture, Equation 2-18 becomes

$$\frac{\partial V_m}{\partial P} = -A\left(\frac{dM}{dt}\right)^{-1} \tag{2-19}$$

or

$$\frac{\partial V_m}{\partial P} = -\frac{1}{G_c} . \tag{2-20}$$

Upon substitution of Equation 2-17 into Equation 2-20 and multiplying both sides of the resulting equation by $\rho_m V_m$,

$$\rho_m V_m G_c = \frac{\rho_m}{V_m}\frac{\partial P}{\partial \rho_m}\rho_m V_m \tag{2-21}$$

which simplifies, by using Equation 2-15 and canceling terms, to

$$G_c^2 = r_m^2 \frac{\partial P}{\partial r_m}. \tag{2-22}$$

Note that

$$v_m = \frac{1}{r_m} \quad \text{and} \quad \partial v_m = -\frac{1}{r_m^2}\partial r_m \tag{2-23}$$

which allows Equation 2-22 to become

$$G_c^2 = r_m^2 \frac{\partial P}{\partial v_m}\frac{\partial v_m}{\partial r_m} = r_m^2 \frac{\partial P}{\partial v_m}\left(-\frac{1}{r_m^2}\right) = -\frac{\partial P}{\partial v_m} \tag{2-24}$$

or

$$G_c = \sqrt{-\frac{1}{\left(\frac{\partial v_m}{\partial P}\right)}}. \tag{2-25}$$

Given the Maxwellian equation

$$\left(\frac{\partial s}{\partial v}\right)_T = \left(\frac{\partial P}{\partial T}\right)_{\cancel{V}} \tag{2-26}$$

and the assumption

$$\left(\frac{\partial P}{\partial v}\right)_{sat} \neq f(\cancel{V}), \tag{2-27}$$

where "sat" refers to saturated conditions and $f(\cancel{V})$ is an arbitrary function of volume, the following is obtained:

$$\partial s = \left(\frac{\partial P}{\partial T}\right)_{sat} \partial v. \tag{2-28}$$

Integrating Equation 2-28 over the two-phase region yields

$$s_{fg} = \left(\frac{\partial P}{\partial T}\right)_{sat} v_{fg}. \tag{2-29}$$

Given the relation

$$Tds = dh - vdP \tag{2-30}$$

and noting that P is constant in the two-phase (saturated) region, the equation

$$Tds = dh \tag{2-31}$$

can be integrated over the two-phase region to yield

$$T_{sat} s_{fg} = h_{fg} . \tag{2-32}$$

Equation 2-32 can be substituted into Equation 2-29 to obtain the Clausius-Clapeyron relation,

$$\left(\frac{\P P}{\P T} \right)_{sat} = \frac{h_{fg}}{T_{sat} v_{fg}} . \tag{2-33}$$

Now consider

$$\frac{\P v_m}{\P P} = \frac{\P}{\P P}(v_f + x v_{fg}) = \frac{\P v_f}{\P P} + x \frac{\P v_{fg}}{\P P} + v_{fg} \frac{\P x}{\P P} \tag{2-34}$$

and note that $\frac{\P v_{fg}}{\P P}$ is negligible, so that

$$\frac{\P v_m}{\P P} = v_{fg} \frac{\P x}{\P P} = v_{fg} \frac{\P}{\P P} \left[\frac{c_p (T_o - T_{sat})}{h_{fg}} \right]. \tag{2-35}$$

If the stagnation conditions are assumed to be saturated and the expansion to be isentropic, Equation 2-35 becomes

$$\frac{\P v_m}{\P P} = - \frac{v_{fg}}{h_{fg}} c_p \frac{\P T_{sat}}{\P P} . \tag{2-36}$$

By using Equations 2-33 and 2-25, it is apparent that

$$\frac{\P v_m}{\P P} = -c_p T_{sat} \frac{v_{fg}^2}{h_{fg}^2} \tag{2-37}$$

and

$$G_c = \frac{h_{fg}}{v_{fg}} \sqrt{\frac{1}{c_p T_{sat}}} . \tag{2-38}$$

Equation 2-38 is the well known Equilibrium Rate Model (ERM) [4] where h_{fg} and v_{fg} refer respectively to the latent heat of vaporization $\left(h_g - h_f\right)$ and the change in specific volume across the entire saturation line $\left(v_g - v_f\right)$ corresponding to an absolute saturated receiver temperature, $T_{sat}\ \left(^oK\right)$. The specific heat of the saturated liquid, c_p, corresponds to the same saturation temperature.

Hans Fauske [4] proposed a modification of the ERM that is useful for the prediction of the non-equilibrium region, and produced the Relaxation Length Model (RLM). In this region the flow increases dramatically as the duct length decreases — approaching all liquid flow as the length approaches zero (i.e., orifice flow). The choked flow, G_{RLM}, is defined by the following in the absence of significant friction losses:

$$G_{RLM} = \frac{h_{fg}}{v_{fg}}\left(\frac{1}{NTc_p}\right)^{1/2}. \tag{2-39}$$

The non-equilibrium number, N, is defined by

$$N = \left(\frac{h_{fg}}{v_{fg}}\right)^2\left[\frac{v_f}{2\Delta PK^2c_pT}\right] + \frac{l_w}{l} \tag{2-40}$$

where K is the resistance coefficient and v_f is the saturated liquid specific volume at temperature T. Fauske determined a critical duct length, l, to be 0.1 meters. As the duct length, l_w approaches the critical length, the value of N approaches a value of one, which corresponds to equilibrium flow conditions. When N equals one, the above equation becomes the well-known ERM that has an alternate form,

$$G_{ERM} = \frac{dP}{dT}\left(\frac{T}{c_p}\right)^{1/2}. \tag{2-41}$$

Another variation of the RLM occurs when the duct length equals zero. This implies no flashing occurring through the break and the RLM equation simplifies to the well known Orifice Equation Model (OEM) for incompressible liquid flow as follows [4]:

$$G_{OEM} = 0.61\sqrt{\frac{2\Delta P}{v_f}} \,. \qquad (2\text{-}42)$$

A comparison of the HEM, ERM and OEM (Figure 2-3) demonstrates the effect of an increasing duct length, l_w, resulting in the choked flow approaching an asymptotic value corresponding to equilibrium flow conditions. In other words, the flow behavior is obviously less sensitive to an increase in the duct length when the critical length is reached.

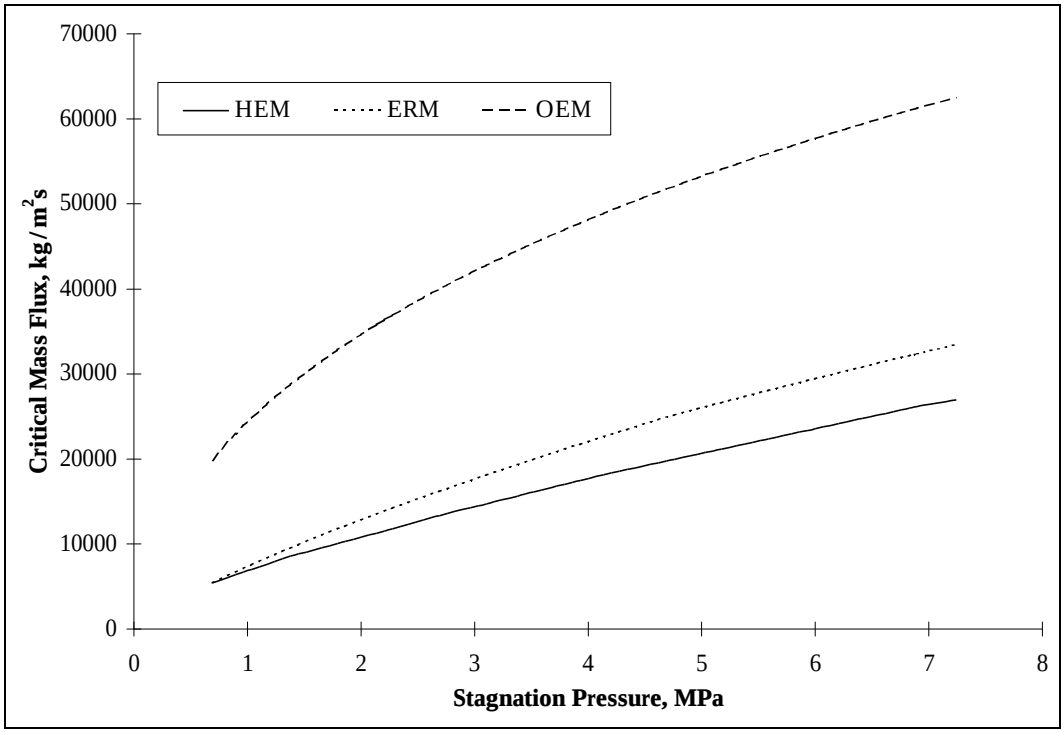

Figure 2-3. Critical mass flux for initially saturated water calculated by analytical models: Homogeneous Equilibrium Model, Equilibrium Rate Model, and Orifice Equation Model.

2.3 Low Flow Quality

Since its inception into the mainstream of two-phase critical flow analyses, the HEM has been shown to severely under-predict the experimental data for low vapor quality [5]. Henry and Fauske developed the following transcendental expressions, often called the Henry-Fauske Subcooled Model (HFSM), for subcooled and saturated liquid stagnation conditions [6]:

$$G_c^2 = \left\{ (v_g - v_{fo}) \frac{(1-x_o)N_s}{s_{gE} - s_{fE}} \frac{ds_{fE}}{dP} \right\}_t^{-1} \tag{2-43}$$

$$\frac{P_t}{P_o} = 1 - \frac{v_{fo} G_c^2}{2P_o}. \tag{2-44}$$

Experimental analysis yielded the approximation

$$N_s = \begin{cases} \frac{x_{Et}}{0.14} & \text{for } x_{Et} \le 0.14 \\ 1 & \text{for } x_{Et} > 0.14 \end{cases}. \tag{2-45}$$

The subscript, E, refers to a fluid state in which the phases are in velocity, temperature and free-energy equilibrium. The conditions at the nozzle's throat, denoted by the subscript t, are considered to be at this equilibrium state. The HFSM predicts the data reasonably well throughout the reported ranges of pressures and subcoolings.

3. APEX Test Facility Description

The OSU APEX test facility is a one-fourth height, one-half time scale, reduced pressure integral systems facility. A formal scaling analysis [9] has been performed to assure that it accurately models the details of the AP600 geometry including the primary system, the passive safety systems, and parts of the non-safety grade Chemical and Volume Control System (CVS) and Residual Heat Removal System. The geometry of the interconnecting pipe routings are also duplicated. All of the primary system components are fabricated of stainless steel and are capable of prolonged operation at 2760 kPa (400 psia) and saturation conditions.

Because data from the facility will be used as part of the AP600 certification process, the applicable sections of ASME NQA-1 have been satisfied [10]. In particular, requirements for instrument calibration and records have been established in accordance with Appendix B of Title 10 Part 50 of the Code of Federal Regulations [11]. Quality assurance (QA) procedures were implemented in accordance with the Project Quality Plan [12]. Facility audits were performed by the NRC, Westinghouse QA, and the U.S. Department of Energy. Numerous safety audits were performed by national, state and local safety and licensing agencies. General layouts of the APEX facility are presented in Figure 3-1 through Figure 3-3.

3.1 APEX Primary System

The APEX test facility primary system includes the following components:

- A *Reactor Pressure Vessel* models the upper and lower reactor internals, the core barrel, the downcomer and the core. Connections for the hot and cold legs and direct vessel injection (DVI) lines are provided. The reactor vessel houses 48 electric heater rods each having a 2.54 cm (1 inch) diameter and a heated length of 91.4 cm (36 inches). The maximum core power is 600 kW (2.05 MBtu/hr).

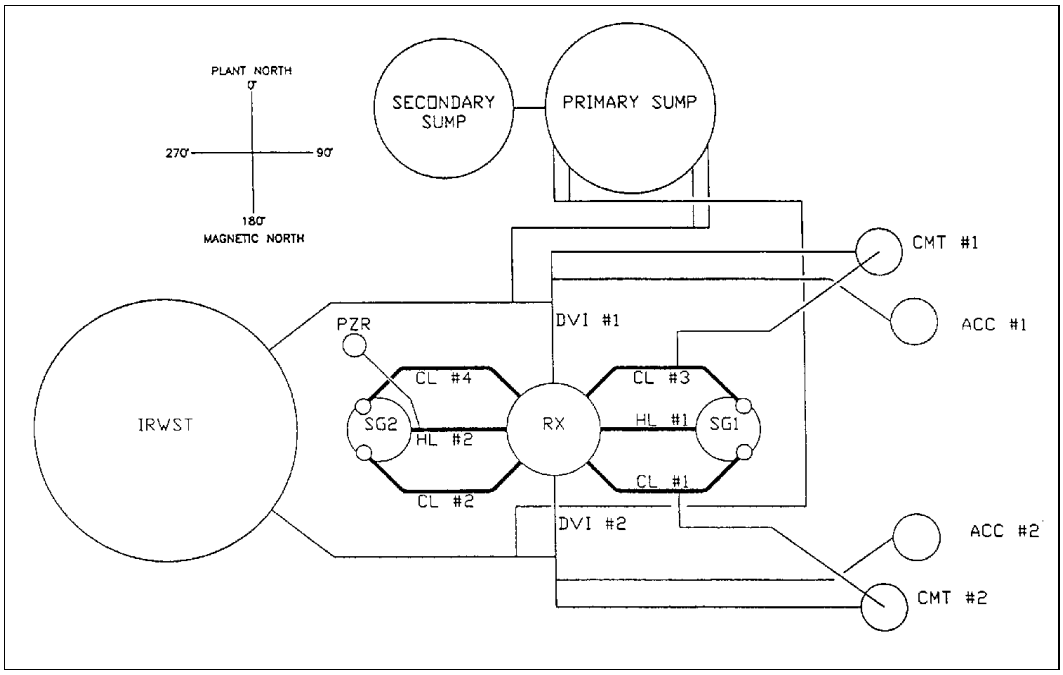

Figure 3-1. APEX Test Facility Line Diagram.

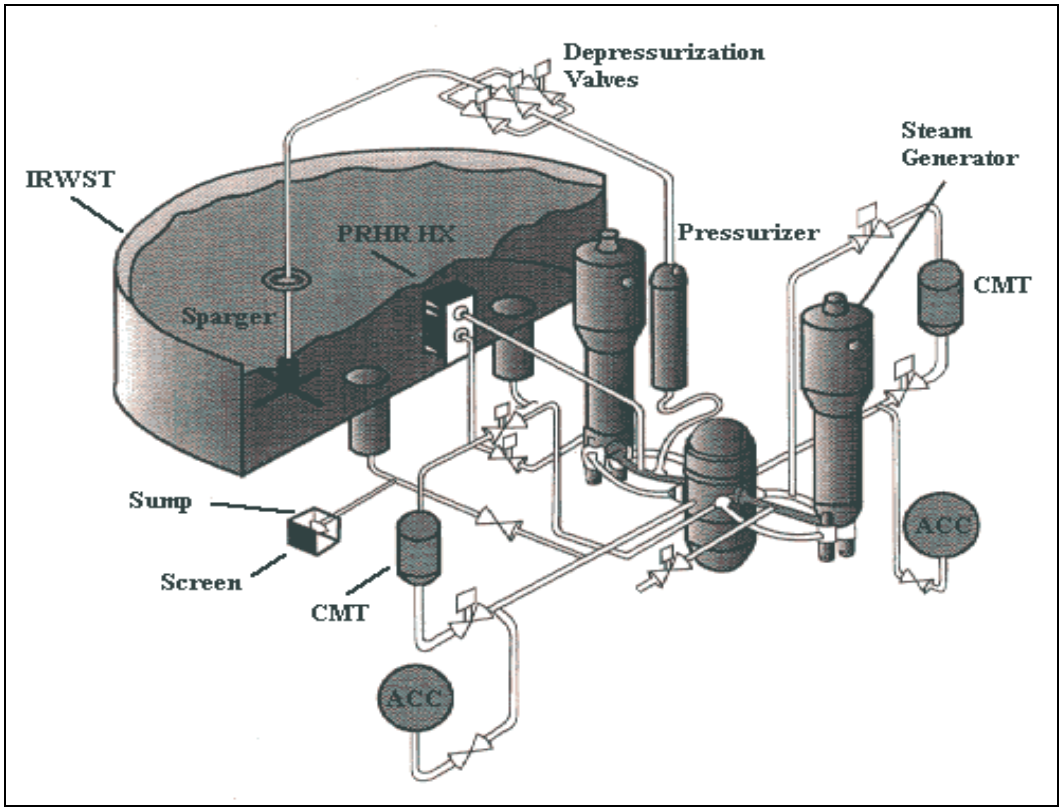

Figure 3-2. APEX Test Facility Layout Diagram.

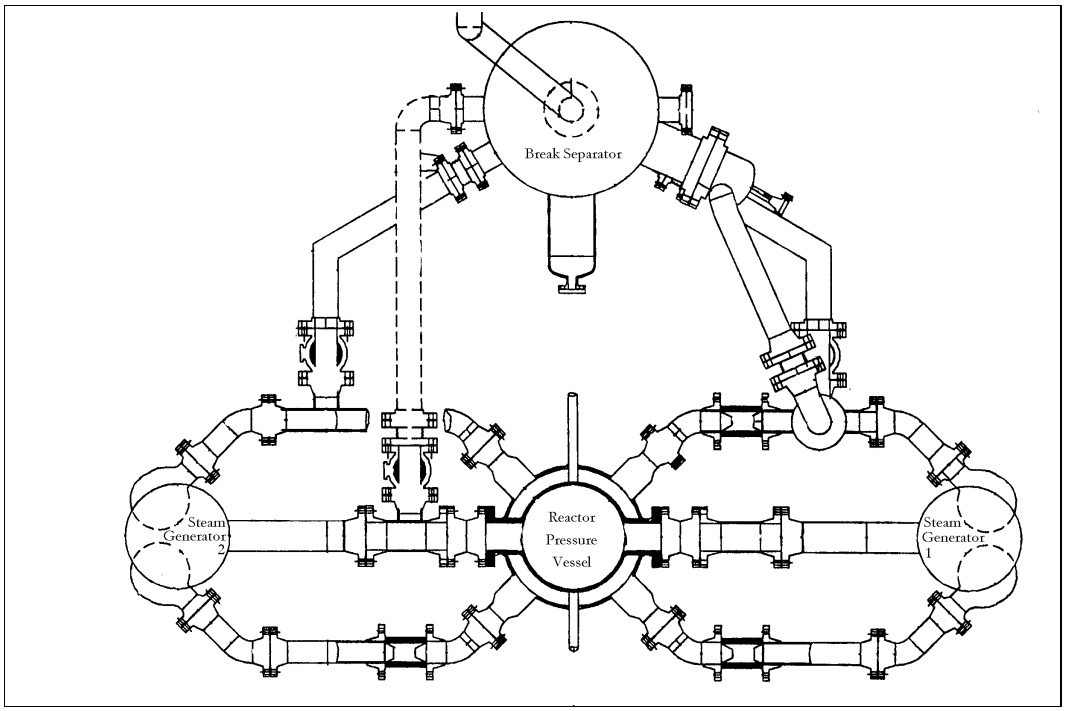

Figure 3-3. Break simulation piping arrangements – overhead view – including Break Separator, Reactor Pressure Vessel, Steam Generators 1 and 2, and various pipe and break spool configurations.

- *Reactor Coolant Loop Piping* models two primary loops, each consisting of one hot leg and two cold legs. Break spool pieces are installed on the hot and cold legs, the DVI line, and the CMT pressure balance line (CMT-PBL) to simulate pipe breaks. The discharge from these valves vent to the Break and ADS Measurement System (BAMS). The BAMS system is used to measure break flow rates.

- Two *Steam Generators (SGs)* , one on each loop, have tube and shell dimensions scaled to simulate Westinghouse Delta-75 steam generators.

- Four *Reactor Coolant Pumps (RCPs)* are used – two attached to the lower channel head of each steam generator.

- A *Pressurizer (PZR)* has internal heaters capable of controlling pressure and minimizing pressure spikes in the reactor coolant system.

3.2 APEX Passive Safety System

The APEX test facility includes the following passive safety systems:

- Two *Core Makeup Tanks (CMTs)* each have a pressure balance line that connects the CMT head to the cold leg. Each CMT also has an injection line that permits draining of the CMT into one of two Direct Vessel Injection (DVI) Lines connected to the reactor downcomer. Check valves and isolation valves have been included.

- An *In-Containment Refueling Water Storage Tank (IRWST)* has two injection lines that connect to the DVI lines. The IRWST is capable of being pressurized to 550 kPa (80 psia) to simulate containment back-pressure.

- An *Automatic Depressurization System (ADS)* includes three valves on the top of the PZR. The flow from these valves are vented to a sparger inside the IRWST. The ADS1-3 Flow nozzles are sized to represent two-trains of the AP600 ADS1-3. The fourth stage of the ADS is modeled by a single valve located on the top of each of the hot legs. The ADS flow nozzles are sized to model two trains of ADS 4 on each hot leg. The fourth stage ADS flows are vented into the primary sump.

- Two *Accumulators (ACCs)* pressurized with nitrogen provide safety injection during depressurization events. Each accumulator has an injection line that connects to one of the two DVI lines.

- A *Passive Residual Heat Removal (PRHR)* heat exchanger is located inside the IRWST. The PRHR is a passive natural circulation heat exchanger which draws water from a hot leg, rejects the heat to the IRWST, and returns the cooled water to the cold leg channel of one steam generator.

3.3 Break and ADS Measurement System

The Break and ADS Measurement System (BAMS) is used to measure two-phase flows from breaks and the four stages of the Automatic Depressurization System (ADS). The two-phase flow is directed to one of four separators where the flow is separated into single phase liquid and single phase vapor. Since the initial liquid level in the break separator is equal to the loop seal

discharge elevation, the liquid entering the break separator will displace liquid in the loop seal. The liquid flow through the loop seal is measured using a magnetic flow meter and directed to the appropriate tank (IRWST or Primary Sump). The vapor flow from the break and ADS 4 is measured with a vortex flow meter and vented from the test facility. Vapor flow from the ADS 1-3 separator is measured and directed into the IRWST. Electrical strip heaters are used to maintain boundary conditions at approximately 93 ºC (200 ºF). The system is capable of being pressurized to 550 kPa (80 psia) to simulate containment back-pressure. As partially shown in Figure 3-4, the BAMS contains the following components:

- A *Primary and a Secondary Sump* simulate the containment compartment volumes below the normal flood-up elevation. The sump tanks are capable of being pressurized to 550 kPa (80 psia) to simulate containment back-pressure. Return lines to the DVI lines are provided to represent the lower containment recirculation lines.

- Four *Moisture Separators* are sized based on maximum expected flow rates. Separation is primarily accomplished by the use of gravity and a swirl vane moisture separator element. Each separator is provided with a loop seal line on the liquid discharge to ensure vapor flow does not bypass the separator.

- *Containment Sump Return System* provides heated water from a hold-up tank to be pumped into the primary sump and the IRWST at a mass flow rate equivalent to the mass flow rate of the vented steam. This heated liquid simulates the flow of condensate from the steam vented into the containment building. This steam would be condensed and drain into the IRWST or the containment (primary) sump.

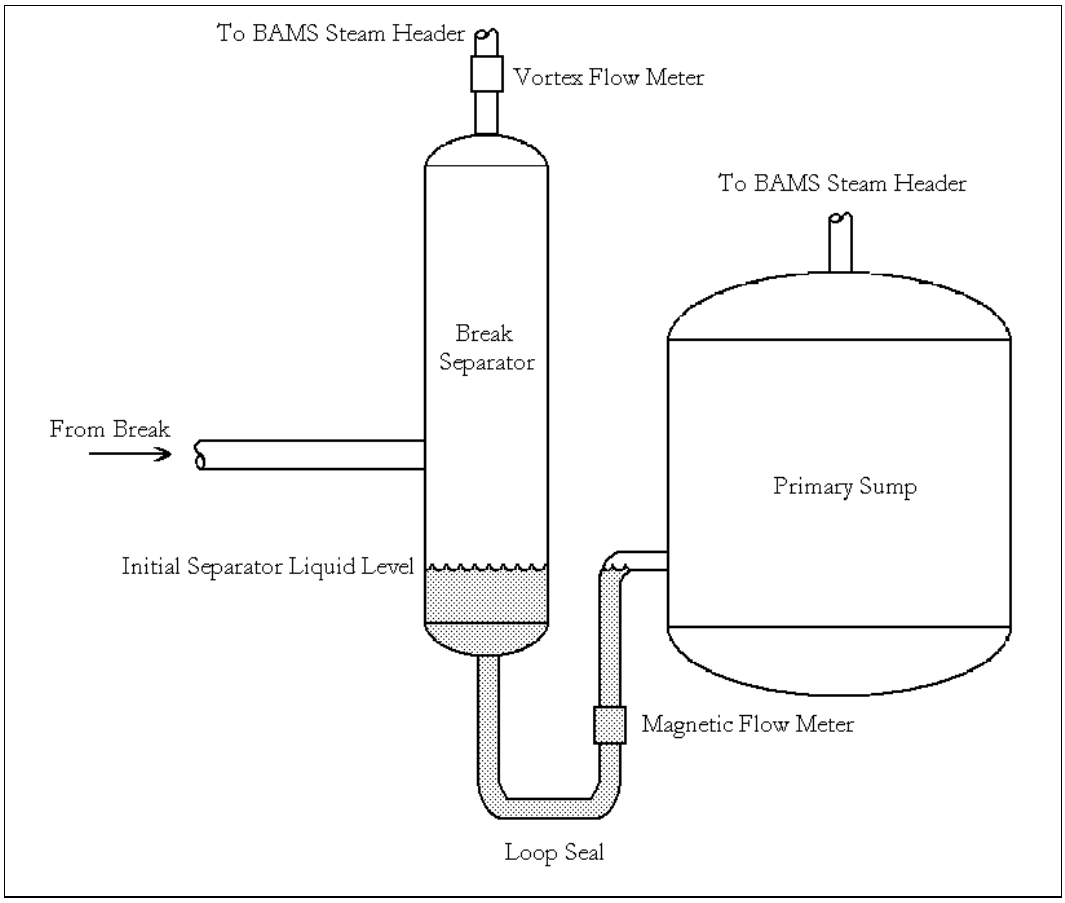

Figure 3-4. BAMS general layout for break flow measurements.

3.4 Instrumentation

Instrumentation is provided to record the necessary data to calculate mass and energy balances. Approximately 750 channels are continuously recorded by the Data Acquisition System (DAS). The APEX test facility includes the following types of instrumentation:

- *Thermocouples* are used to measure the temperature of the coolant in the primary and secondary systems, and the supply and component cooling water systems. They are also used to measure the temperature distribution in the CMT walls and the core heater rods. Premium grade thermocouples have been used and connected to the data acquisition system (DAS) through controlled purity thermocouple wire.

- *Magnetic Flow Meters* are used to measure all single phase liquid flow rates.

- *Pressure Transducers* are used to measure the static pressures within the various tanks and vessels.
- *Differential Pressure transducers* are used to measure the liquid levels in various tanks , vessels, and pipes. They are also used to determine pressure drop in system piping and across various fittings and components.
- *Vortex Flow Meters* are used to measure all vapor flow rates.
- *Heat Flux Meters* are used to measure heat loss from individual tanks and components.
- *Load Cells* are used to measure the weight of liquid inside large tanks.
- Ambient air temperature, humidity and barometric pressure are also recorded.
- All of the instruments are monitored by the DAS which records the data on computer files.

3.5 Data Acquisition and Control

The Data Acquisition and Control System (DAS) includes all the equipment necessary to receive, transmit, process and record the voltage or current signal outputs from the individual sensing instruments. This includes amplifiers, signal conditioners, transmitters, interconnecting wiring, analog to digital converters, interfacing boards, switching panels, computers, displays and other recording devices as needed to access the instruments. The DAS selected for this project is a FLUKE HELIOS system linked to three DEC 486 PC Based computers. A Labview software package to process the incoming data has been developed, validated and fully tested. The DAS is capable of storing and maintaining all data retrieved and recorded during a single test. The DAS includes on-line data graphics for process monitoring and a Compact Disk (CD) Writer which provides for permanent storage of all test data on CD.

APEX includes a fully developed control panel capable of modeling all of the important safety logic of the AP600. All control actions, such as valve openings and closures, pumps starts, and safety signals are monitored and recorded using the WONDERWARE software package (same package used for NASA's space shuttle program). This package provides a time history of all control actions that occur during a test. The WONDERWARE software package has been fully validated and tested.

4. Evaluation of the APEX Break Flow Measurement System During Subcooled Depressurization

The current analysis compares the initial break flow rates measured by the BAMS with those estimated by the initial liquid level depression rate of the pressurizer using data from several OSU APEX Matrix tests. In addition to these data analyses, initial break flow rates are estimated using several well-known critical flow models: HEM, ERM, RLM, HFSM and OEM.

4.1 BAMS Assessment Methodology

Several small break simulations have been performed in the OSU APEX test facility. The tests are initiated from subcooled conditions. That is, the hot leg temperature is usually 215 °C (420 °F) while the system pressure is maintained near 2700 kPa (390 psia). Upon opening the break valve, the system undergoes a brief period of depressurization while at subcooled conditions. For the one inch break simulation, this corresponds to approximately 200 seconds, and for the one-half inch break simulation, this corresponds to approximately 800 seconds. During this period, subcooled critical flow is established at the break, and the break flow is measured by the BAMS. Because there are no other mass losses from the primary system, by using a simple mass balance, the change in liquid level in the pressurizer, $\left(\frac{dL}{dt}\right)_{pzr}$, can be directly related to the break flow rate as

$$G_{Break} \approx -\frac{A_{pzr}\, r_{pzr}}{A_{Break}}\left(\frac{dL}{dt}\right)_{pzr}. \qquad (4\text{-}1)$$

Figure 4-1 shows the pressurizer liquid level as a function of time for test NRC-5001 [13]. The slope, $\left(\frac{dL}{dt}\right)_{pzr}$, of the pressurizer liquid level with respect to time (Figure 4-1) is determined to be $-5.62 \cdot 10^{-3}$ m/s. Substituting the values for the slope, the break cross-sectional flow area, the pressurizer liquid density and the pressurizer cross-sectional flow area into Equation 4-1 yields an estimate of 25884 kg/m^{2}s for the critical flow rate at the break. Table 4-1 presents similar comparisons for several of the small break simulations. The uncertainties associated with the pressurizer liquid level measurements are discussed in Section 4.4.

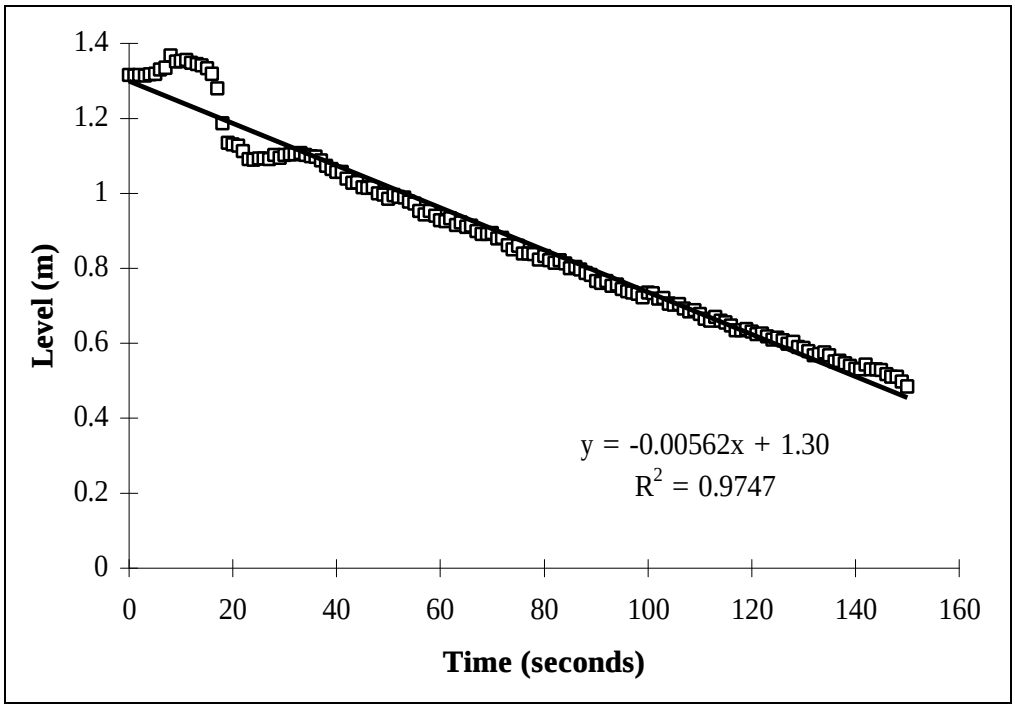

Figure 4-1. NRC-5001 [13] pressurizer liquid level as a function of time during subcooled blowdown.

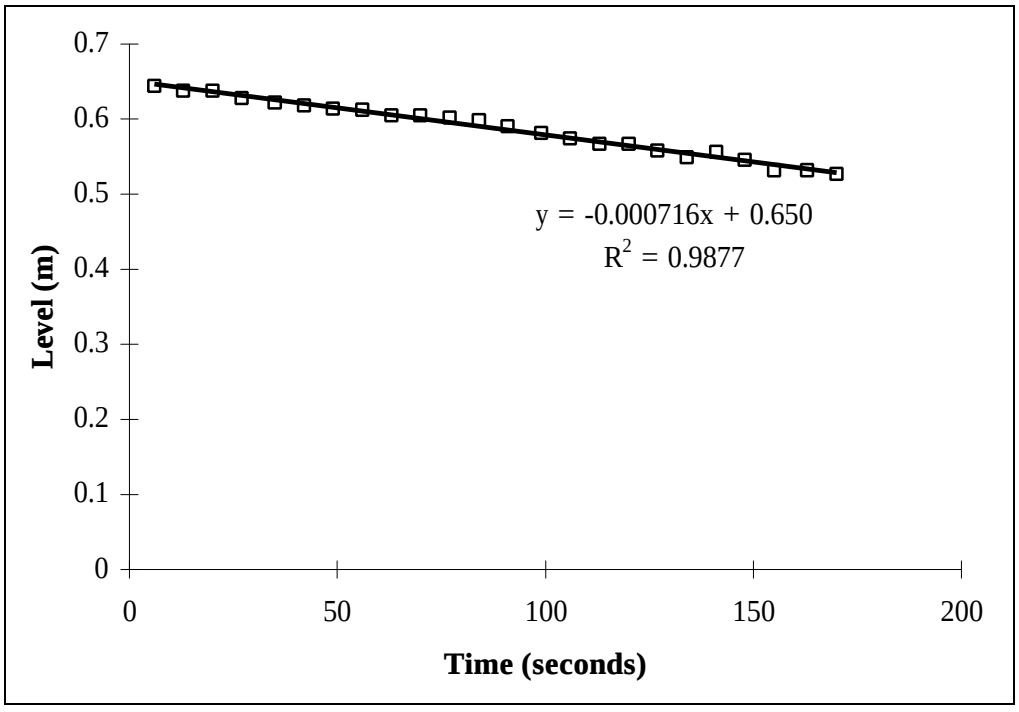

Figure 4-2. NRC-5005 [14] pressurizer liquid level as a function of time during subcooled blowdown.

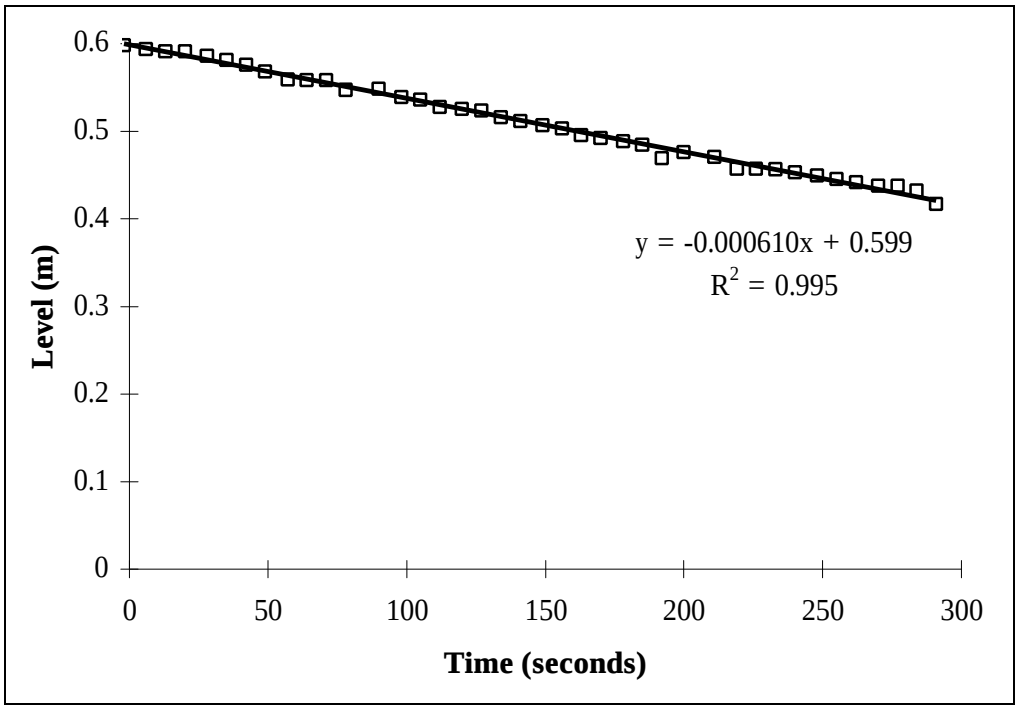

Figure 4-3. NRC-5105 [15] pressurizer liquid level as a function of time during subcooled blowdown.

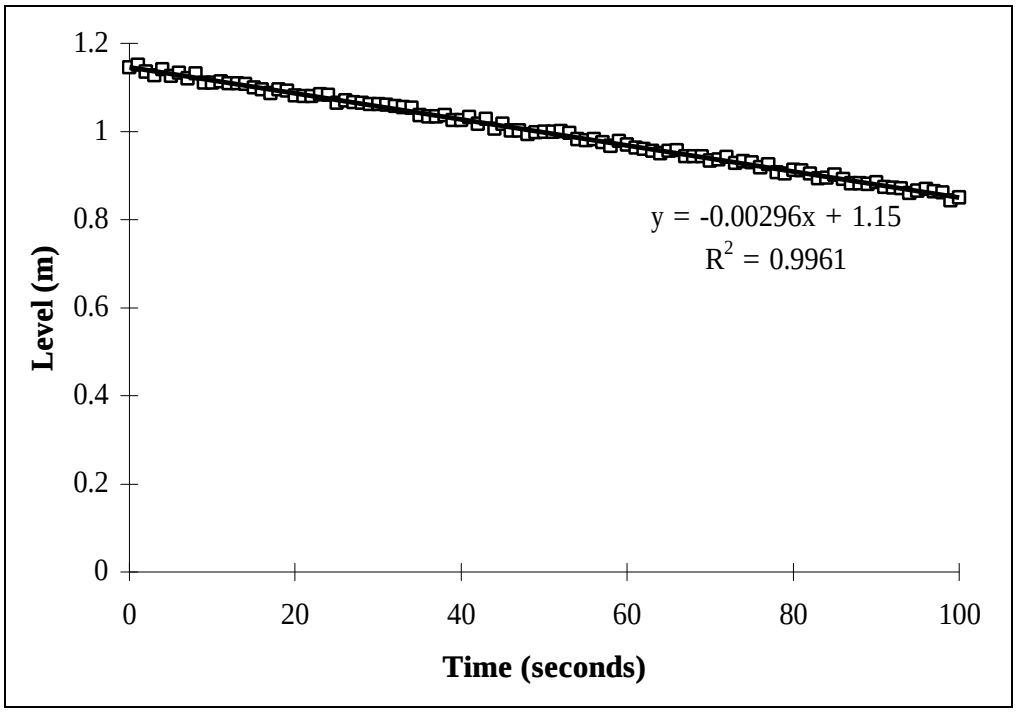

Figure 4-4. NRC-5007 [16] pressurizer liquid level as a function of time during subcooled blowdown.

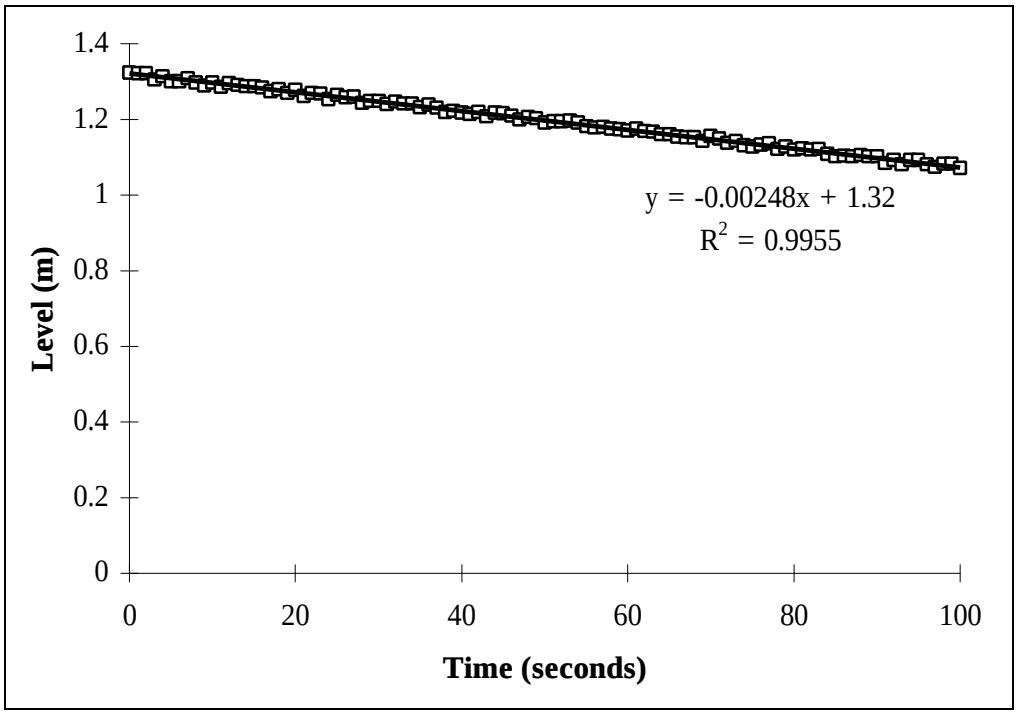

Figure 4-5. NRC-5107 [17] pressurizer liquid level as a function of time during subcooled blowdown.

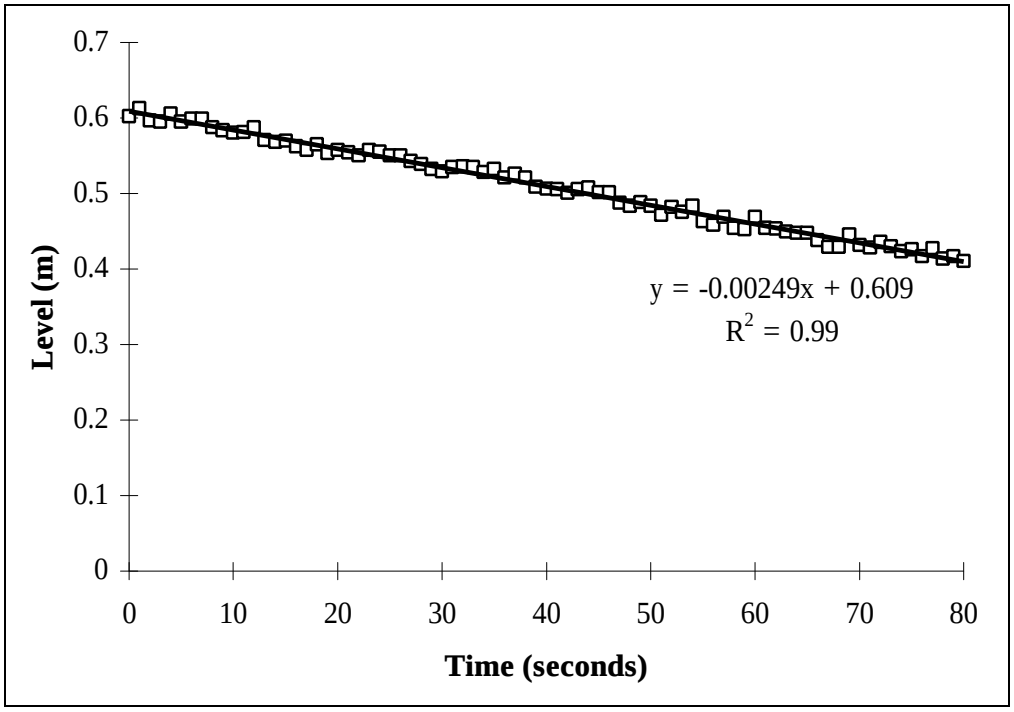

Figure 4-6. NRC-5010 [18] pressurizer liquid level as a function of time during subcooled blowdown.

In addition to comparing the measured flow rates to the pressurizer level data, it is also insightful to determine which critical flow correlations best describe the measured data. It should be noted that the break nozzles implemented in the test were designed to simulate the ratio of the actual AP600 pipe wall thickness to the break hole diameter (L/D). As such, the usual assumption of homogeneous equilibrium conditions (i.e., $L/D \geq 40$) would not be applicable. Table 4-2 lists the initial mass flux predictions of several well-known critical flow correlations.

4.2 Results of BAMS Assessment

The assessment of the BAMS included a quantification of the observed measurement delay. This time delay is discussed in greater detail in Section 0. As discussed in Section 4.1, a comparison of the BAMS initial flow rate measurements to calculations using Equation 4-1 is also summarized. The initial mass flux predictions of the critical flow models described in Chapter 2 are listed for comparison to the BAMS initial mass flux data. The results of the BAMS assessment are given in Table 4-1 and Table 4-2 below.

Table 4-1. Test data results from pressurizer level and BAMS break flow measurements.

Test ID	$\frac{A_{pzr}}{A_{Break}}$	*BAMS Time Delay (seconds)*	*BAMS Initial Mass Flux Data (kg/m2s)*	*Pressurizer* $\left(\frac{dL}{dt}\right)_{pzr}$ *(m/s)*	*Mass Flux Using Equation 4-1 (kg/m2s)*
NRC-5001 [13]	5539.3	68	28865	$-5.62 \cdot 10^{-3}$	25884
NRC-5003 [19]*	1384.8	77	31392	–	–
NRC-5005 [14]	50735.4	134	27500	$-7.16 \cdot 10^{-4}$	30196
NRC-5105 [15]	50735.4	28	28003	$-6.10 \cdot 10^{-4}$	25699
NRC-5007 [16]	12612.4	153	34887	$-2.96 \cdot 10^{-3}$	31016
NRC-5107 [17]	12612.4	99	30809	$-2.48 \cdot 10^{-3}$	25983
NRC-5010 [18]	12612.4	115	31176	$-2.49 \cdot 10^{-3}$	26115
NRC-5111 [20]*	1384.8	73	31992	–	–
NRC-5012 [21]*	1384.8	80	27105	–	–

* The level-depression rate within the pressurizer was immeasurable, so it and its corresponding mass flux calculation are not determined.

Table 4-2. Several critical flow correlations 'results for comparison with test data results shown in Table 4-1 (kg/m^2s).

Test ID	*HEM*	*OEM*	*ERM*	*RLM*	*HFSM Using T_o and P_o*	*HFSM Using T_{sat} and P_o*
NRC-5001	1366	42637	1273	3150	36669	30083
NRC-5003	1738	41559	1619	4003	34470	29623
NRC-5005	1276	42861	1192	2950	36431	30184
NRC-5105	1265	42862	1179	2918	36801	30167
NRC-5007	1265	42862	1179	2918	36709	30193
NRC-5107	1459	42685	1362	3369	37007	30220
NRC-5010	1548	42487	1445	3573	36673	30154
NRC-5111	1800	41451	1674	4139	34453	29609
NRC-5012	1191	42572	1109	2745	35010	29740

Several conclusions can be drawn from Table 4-1 and Table 4-2. First, for the same set of initial conditions, the BAMS initial mass flux measurements are consistent, within 7.9 percent, for all the tests listed in Table 4-1. That is, the initial critical break mass flux measured by the BAMS was 30192 ± 2390 kg/m^2s for similar initial conditions. The standard deviation, 2390 kg/m^2s, corresponds to 7.9 percent of the mean measured mass flux. Second, the BAMS measurements are in good agreement with the estimates provided by Equation 4-1. The pressurizer initial break mass flux approximations made by Equation 4-1 yielded a prediction of 27482 ± 2225 kg/m^2s, which under-predicts the BAMS mean mass flux by 9.0 percent and demonstrates the pressurizer liquid level measurements to be repeatable within 8.1 percent. Last, comparisons of the BAMS measurements to the critical flow models indicate that the Henry-Fauske Subcooled Model [6] provides good agreement with the measured data when one uses a saturated temperature, T_{sat}, at the given system pressure, P_o. Since the HFSM was developed for saturated and subcooled liquid system conditions, this is a valid assumption (see Section 2.3). The HFSM over-predicts the BAMS mean mass flux by 19.3 percent when a subcooled pressure and temperature are used. The HFSM using a saturated temperature yields an initial critical break mass flux of 29997 ± 245 kg/m^2s, which shows it to under-predict the BAMS mean mass flux by 0.6 percent. All of these averages and standard deviations are summarized in Table 4-3.

Table 4-3. Average values and population standard deviations of selected mass flux data shown in Table 4-1 and Table 4-2.

	BAMS	*Equation 4-1*	*HFSM Using T_0 and P_0*	*HFSM Using T_{sat} and P_0*
Mean (kg/m^2s)	30192	27482	36025	29997
Population Standard Deviation (σ)	2390	2225	997	245
σ is _% of Mean*	7.9	8.1	2.8	0.8
Mean is _% of Mean-BAMS**	100.0	91.0	119.3	99.4

* This percent corresponds to the ratio of the Population Standard Deviation to the Mean for the specified model or measurement.

** This percent corresponds to the ratio of the specified model or measurement Mean flux to the Mean mass flux of the BAMS measurement.

4.3 Effect of BAMS Measurement Delay

Table 4-1 presents the BAMS 'measured delay times for the series of small break tests. The delay times vary significantly with each test, and they are shown in Figure 4-7 through Figure 4-15. The reason for the differences in time delay may be the existence of slight variations in the break separator's initial liquid level. Because the break separator diameter is quite large, small differences in liquid level represent large volumes relative to the volumetric flow rates of small break simulations. That is, for the very low break flow rates encountered in these tests, the time required to fill the break separator to its steady-state discharge level would be significantly different if the initial break separator was not equal to this optimum steady-state discharge level. For example, an initial break separator liquid level difference of 0.85 cm would explain the time delay difference between NRC-5005 [14] and NRC-5105 [15] as listed in Table 4-1. In general, however, the time delays are insignificant relative to the entire depressurization transient.

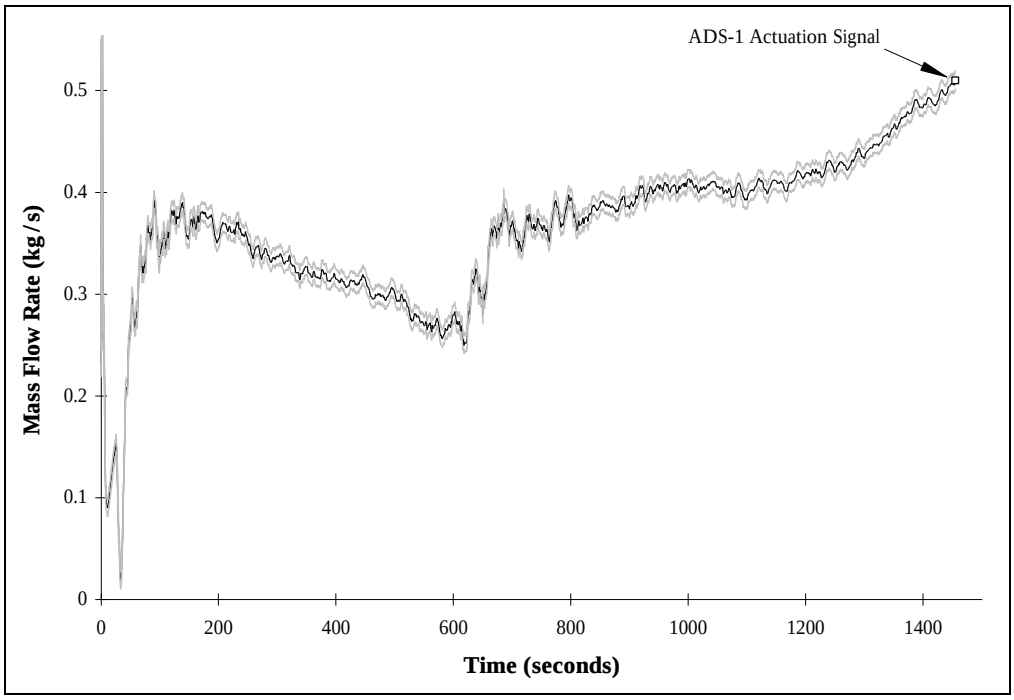

Figure 4-7. NRC-5001 [13] BAMS measured break flow rate and instrumentation uncertainties as functions of time during subcooled blowdown.

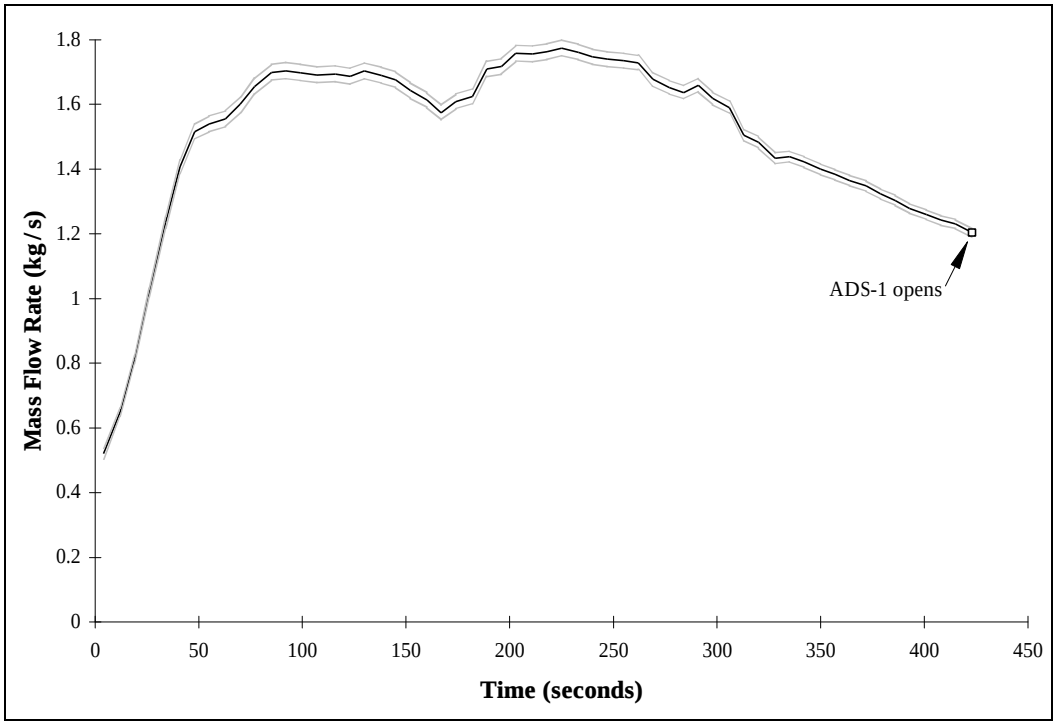

Figure 4-8. NRC-5003 [19] BAMS measured break flow rate and instrumentation uncertainties as functions of time during subcooled blowdown.

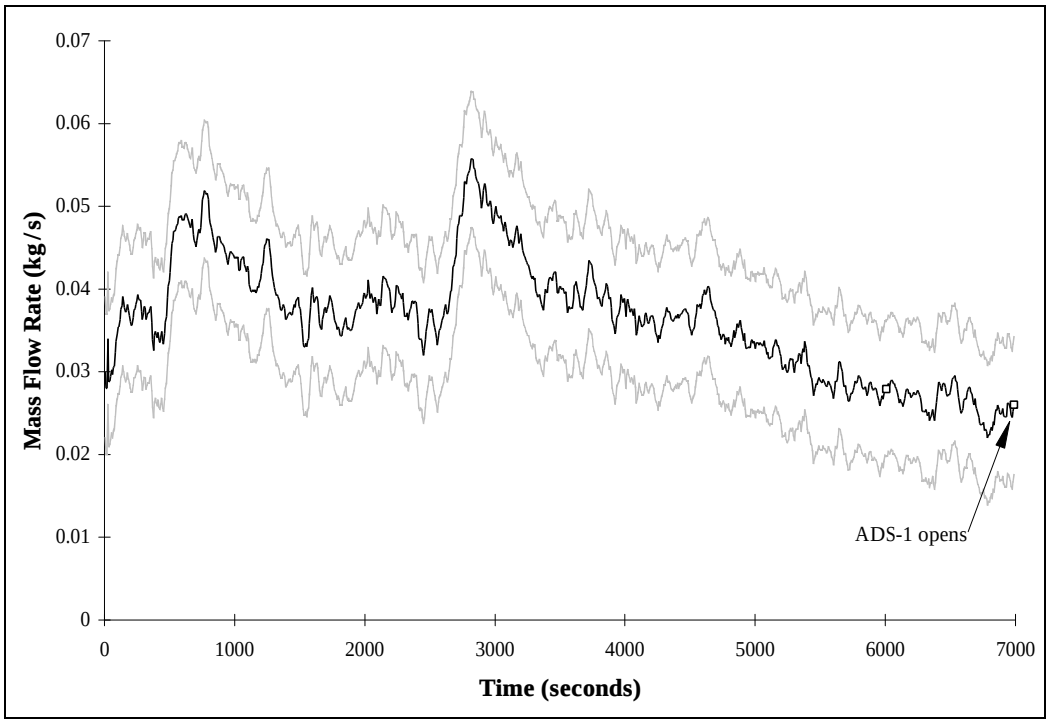

Figure 4-9. NRC-5005 [14] BAMS measured break flow rate and instrumentation uncertainties as functions of time during subcooled blowdown.

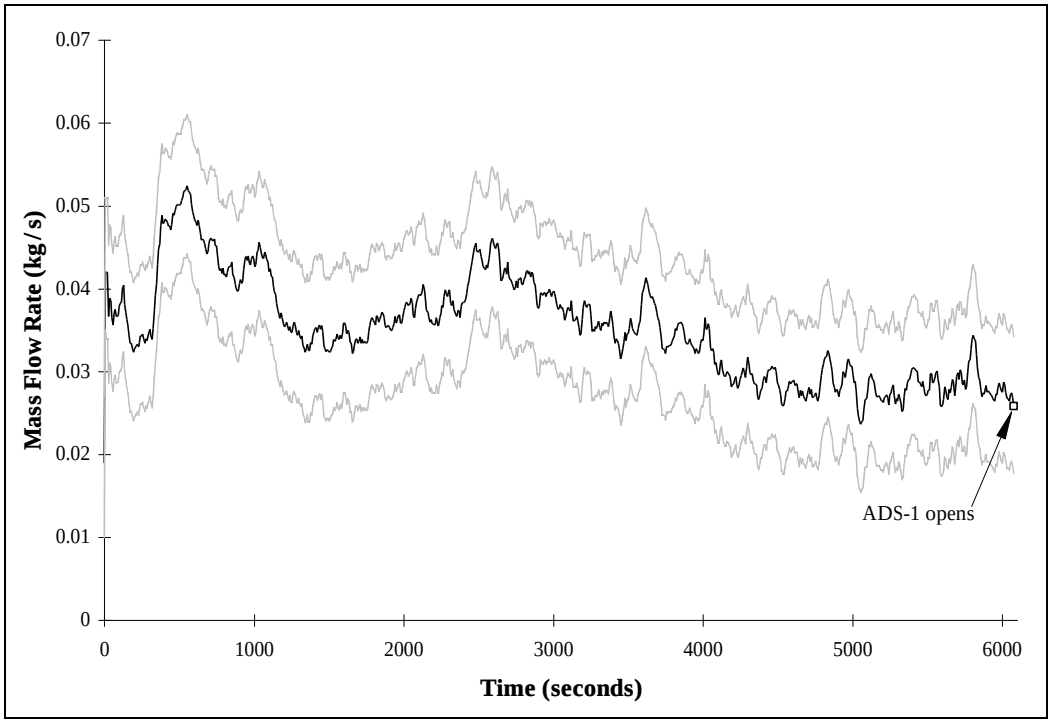

Figure 4-10. NRC-5105 [15] BAMS measured break flow rate and instrumentation uncertainties as functions of time during subcooled blowdown.

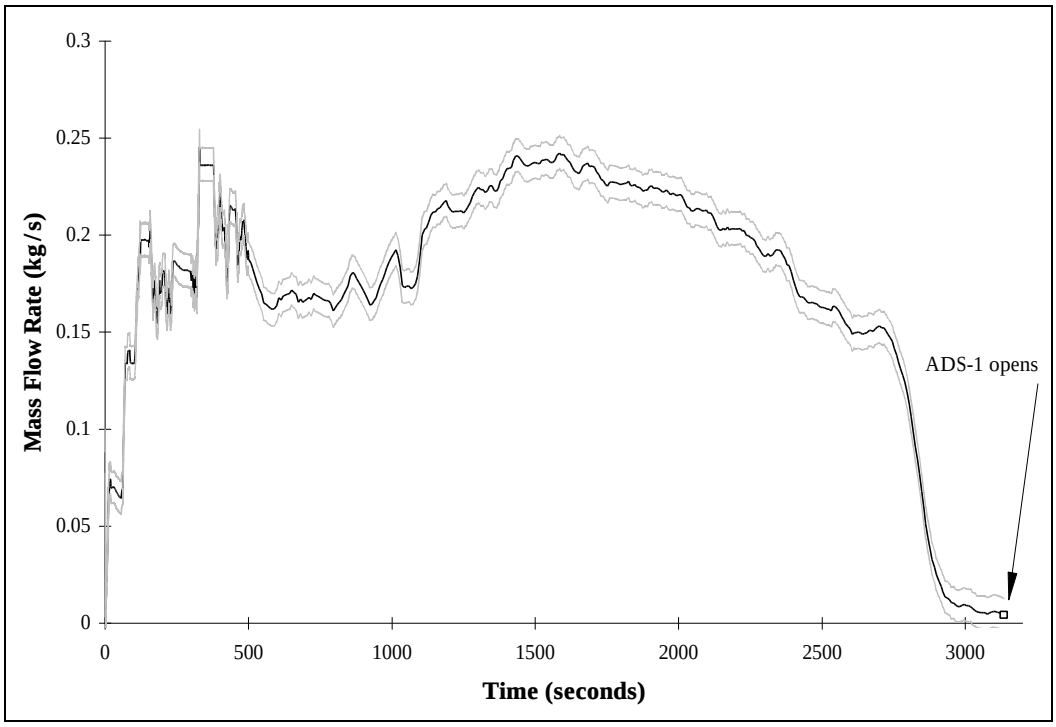

Figure 4-11. NRC-5007 [16] BAMS measured break flow rate and instrumentation uncertainties as functions of time during subcooled blowdown.

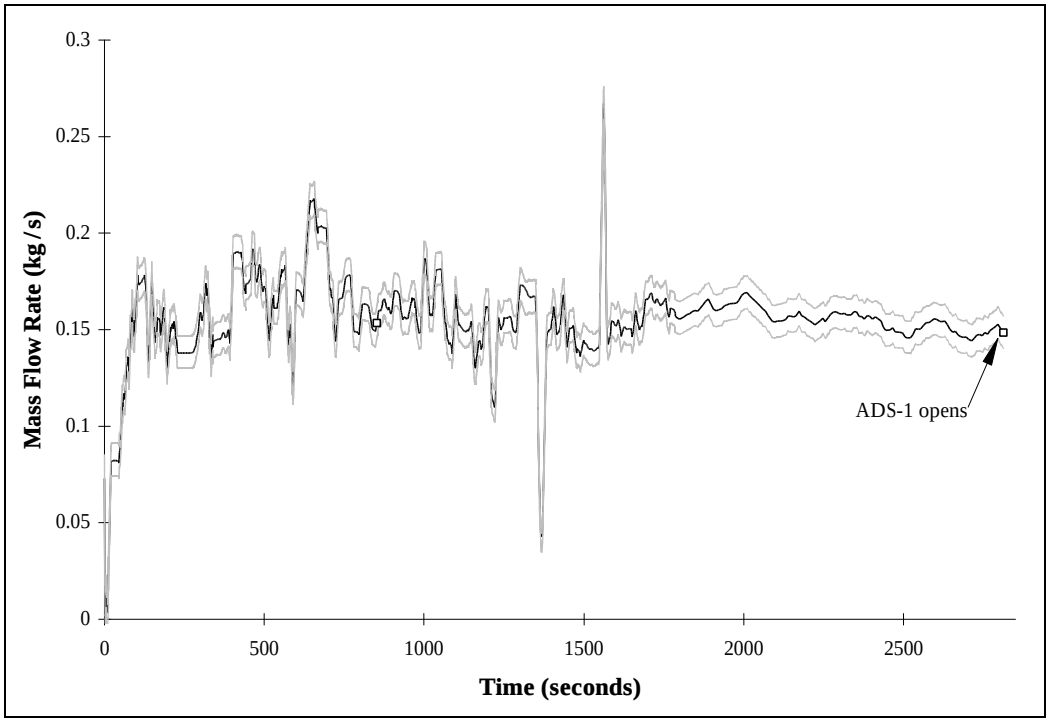

Figure 4-12. NRC-5107 [17] BAMS measured break flow rate and instrumentation uncertainties as functions of time during subcooled blowdown.

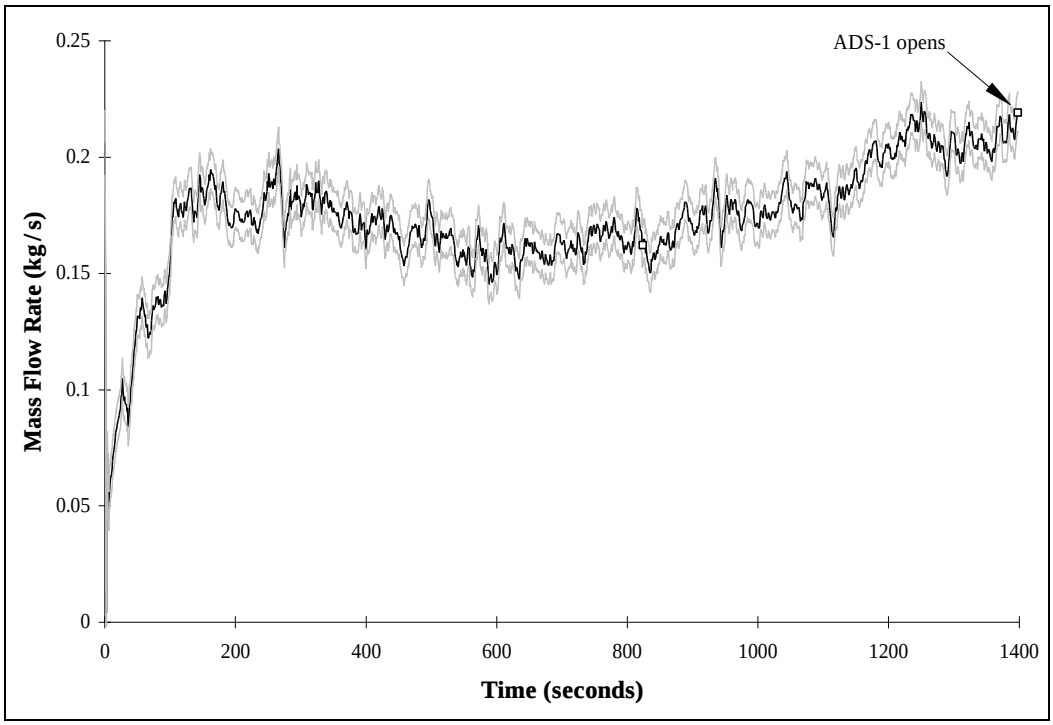

Figure 4-13. NRC-5010 [18] BAMS measured break flow rate and instrumentation uncertainties as functions of time during subcooled blowdown.

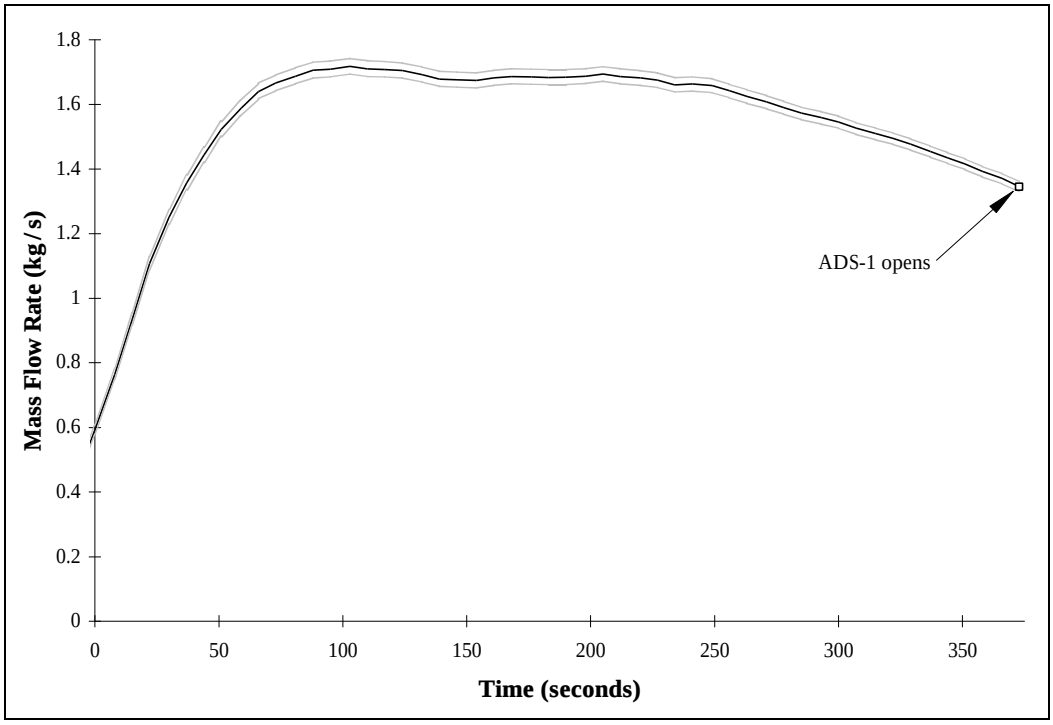

Figure 4-14. NRC-5111 [20] BAMS measured break flow rate and instrumentation uncertainties as functions of time during subcooled blowdown.

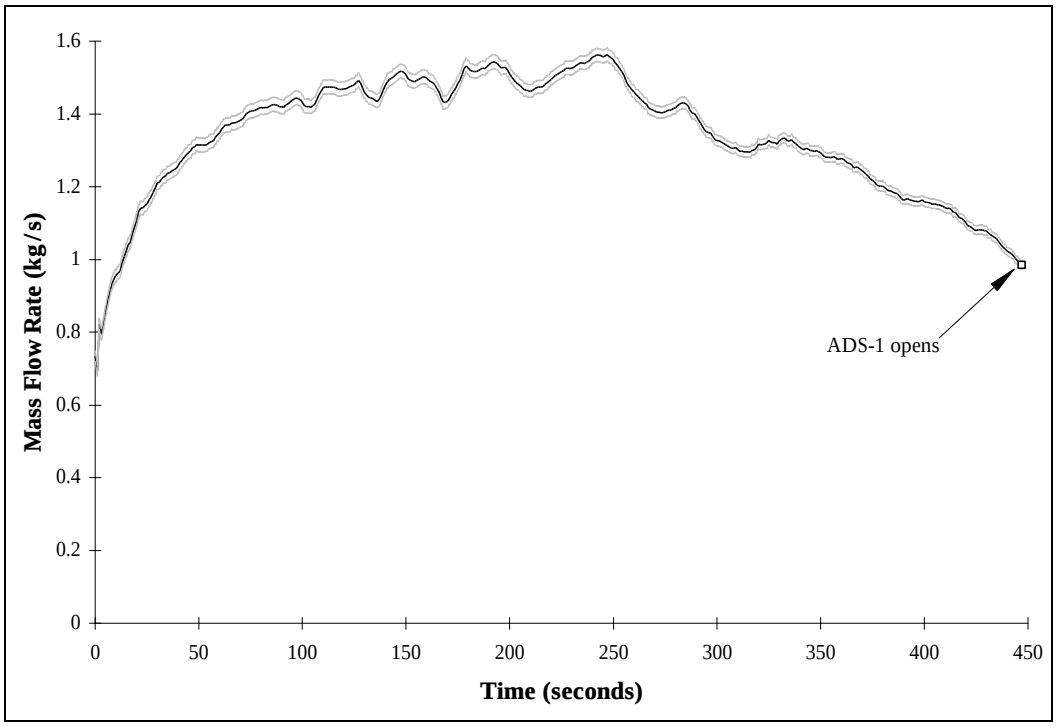

Figure 4-15. NRC-5012 [21] BAMS measured break flow rate and instrumentation uncertainties as functions of time during subcooled blowdown.

4.4 Discussion of Instrumentation Accuracy

As seen in the previous sections, there exists some measurement errors for the instruments used. The *Differential Pressure transducer* used to measure the pressurizer liquid level has an error of ±1.08 cm, and it is not shown in the figures above because it is small compared to the pressurizer's initial liquid level. The error in the level measurement is assumed to be a constant value, since it is based upon a fraction of the transducer's calibrated range. The *Magnetic* and *Vortex Flow Meters* used to measure the liquid and vapor flow rates through the simulated break have errors of ±8.03 cm^3/s and ±950 cm^3/s respectively. The *thermocouple* located in the pressurizer's water-space has an inherent error of ±1.13 °K. All of these instrument errors are taken from the OSU APEX Instrument Calibration Database [22]. When these errors are incorporated into the break flow rate calculations, they yield minimum and maximum flow rates as shown on the figures in the previous section.

5. Integrated Mass Method

Given the above description of the APEX Facility, it is an intuitive assumption that no simple flow model will be adequate to predict the transient break flow behaviors for all possible plant conditions. This assumption leads to the introduction of an integrated method that is not as sensitive to the system's initial conditions.

5.1 Model Description

Because a critical flow condition existed at the break location from the onset of the transient up to the point of ADS-1 actuation, a constant mass flux is assumed from the onset of the transient,

$$G_e = G_0 . \tag{5-1}$$

Also, the discharge coefficient of the break nozzle is assumed to be unity,

$$C_D = 1. \tag{5-2}$$

Using these two assumptions, the integral relationship for the total mass exiting through the break nozzle ,

$$M_e = \int_0^t C_D G_e A_e dt , \tag{5-3}$$

becomes

$$M_e = G_0 A_e t = \dot{m}_0 t . \tag{5-4}$$

Now, define an inverse residence time parameter,

$$w_0 = \frac{\dot{m}_0}{M_0} , \tag{5-5}$$

where $\dot{m}_0$ is the initial mass flow rate through the break and M_0 is the total mass both above the break location and within the pressurized system. Also, the fraction of mass remaining within the system as a function of time is defined as

$$M^* = \frac{M_0 - M_e}{M_0} . \tag{5-6}$$

It is simple to derive a dimensionless group from Equations 5-4 through 5-7 in terms of time and initial conditions only:

$$f = 1 - w_0 t \,. \tag{5-7}$$

Thus, it can be shown that

$$M^* = f \,. \tag{5-8}$$

5.2 Discussion of Results

The dimensionless groups described in the previous section were used to predict the total mass exiting the primary system through the break. The analysis was performed for test times prior the actuation of the ADS for all data, but it should be noted that ADS-1, ADS-2 and ADS-3 valves were not opened during the test, NRC-5001. The BAMS break flow data was integrated and used in Equation 5-6 to determine the time-dependent value of M^*. Then, for the same range of time, *t*, the values of f were calculated using Equation 5-7. Table 5-1 summarizes some important information regarding the results of the aforementioned data analysis, and the data is shown in Figure 5-1 through Figure 5-7. The purpose of the linear regressions is to determine how well the integrated mass model corresponds to the measured data.

Table 5-1. Integrated mass analysis linear data regression information.

Test ID	*Slope*	*Coefficient of Determination,* R^2
NRC-5001	0.9828	0.9844
NRC-5003	1.0021	0.9968
NRC-5105	0.9958	0.9936
NRC-5107	1.0162	0.9904
NRC-5010	1.0053	0.9977
NRC-5111	1.0077	0.9912
NRC-5012	0.9851	0.9952

As can be seen in Table 5-1, the simple integrated mass model yields good predictions of mass losses through the break nozzle to the time of ADS-1 actuation. System conditions change significantly beyond ADS-1 actuation, thus the model would not be valid.

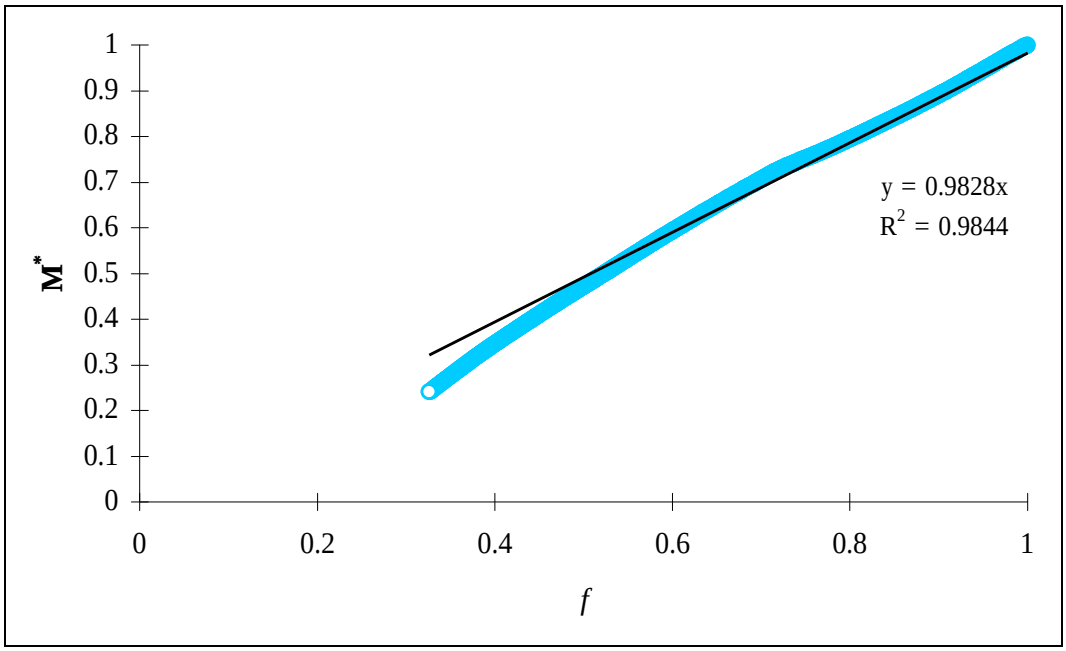

Figure 5-1. NRC-5001 integrated system mass ratio versus integrated flow model dimensionless group.

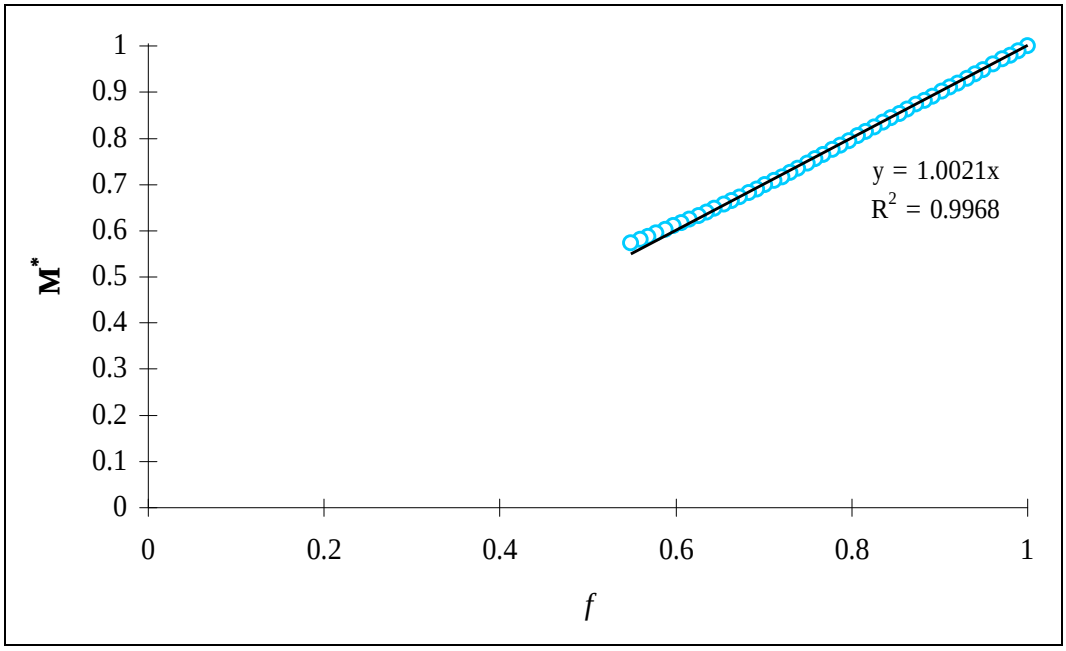

Figure 5-2. NRC-5003 integrated system mass ratio versus integrated flow model dimensionless group.

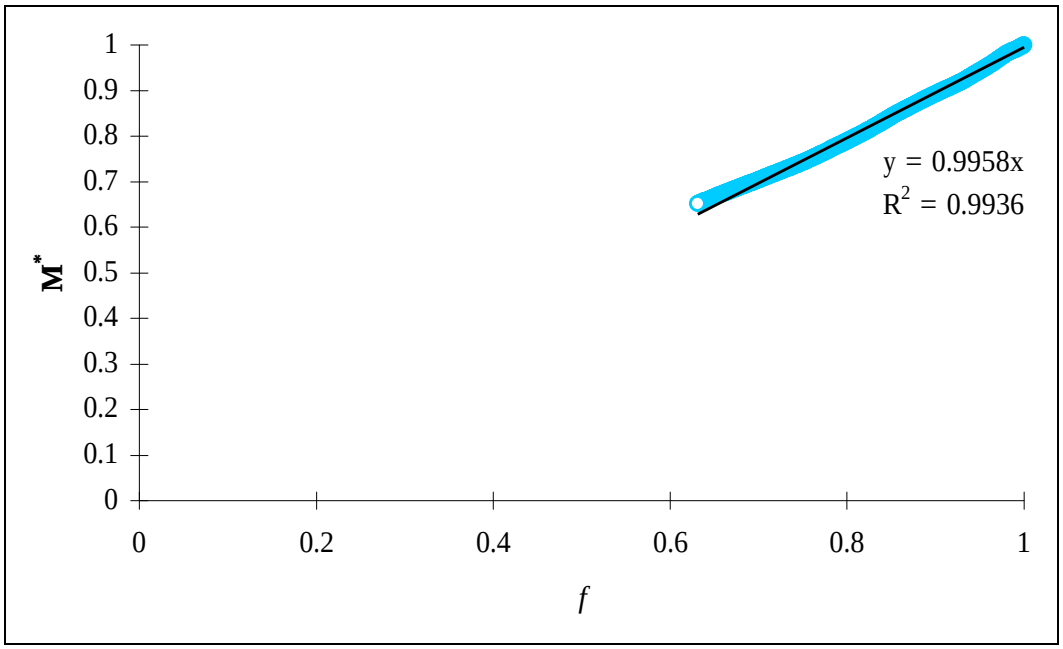

Figure 5-3. NRC-5105 integrated system mass ratio versus integrated flow model dimensionless group.

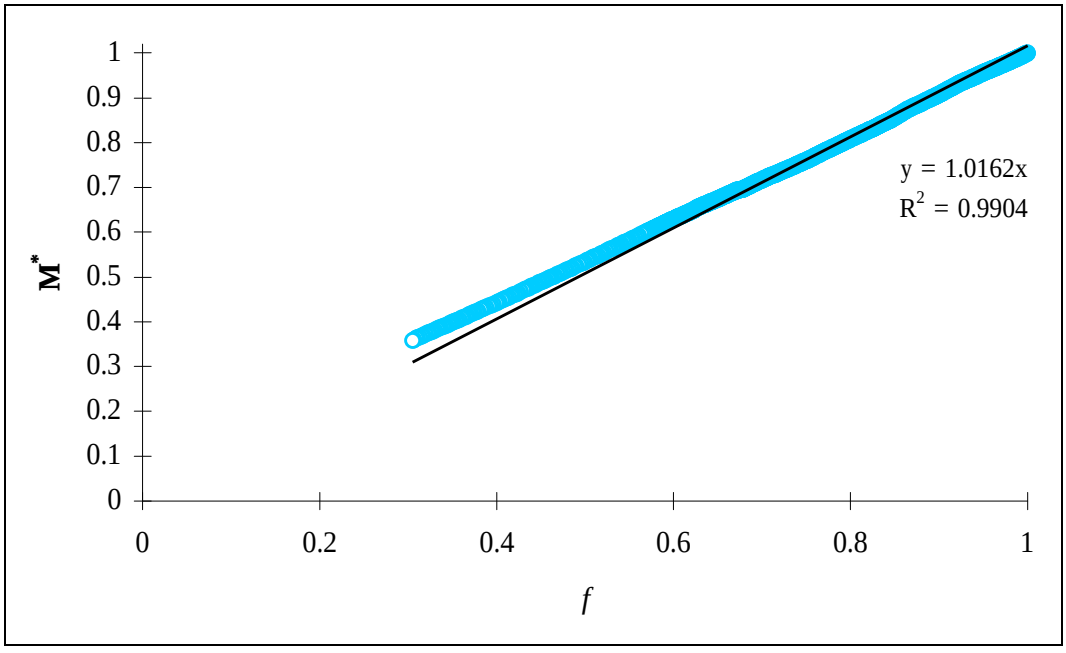

Figure 5-4. NRC-5107 integrated system mass ratio versus integrated flow model dimensionless group.

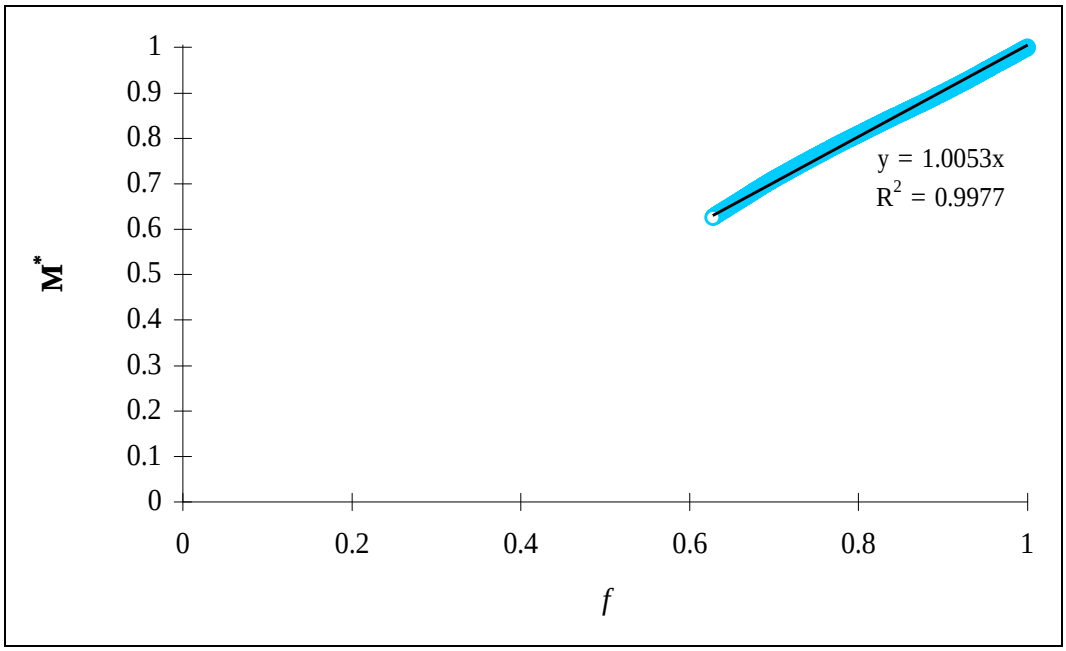

Figure 5-5. NRC-5010 integrated system mass ratio versus integrated flow model dimensionless group.

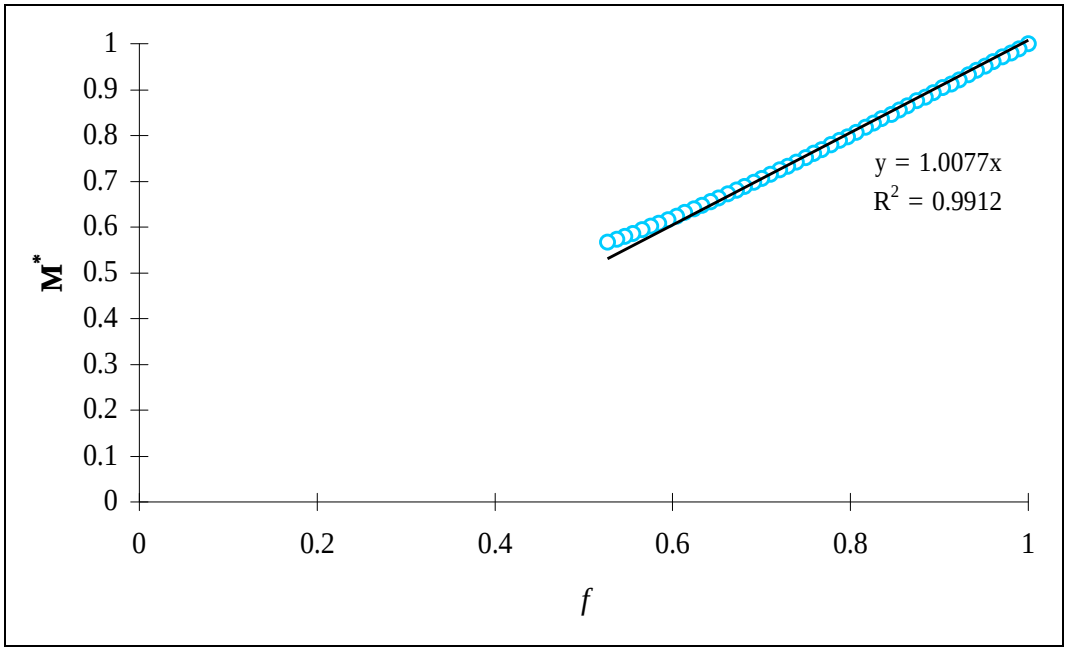

Figure 5-6. NRC-5111 integrated system mass ratio versus integrated flow model dimensionless group.

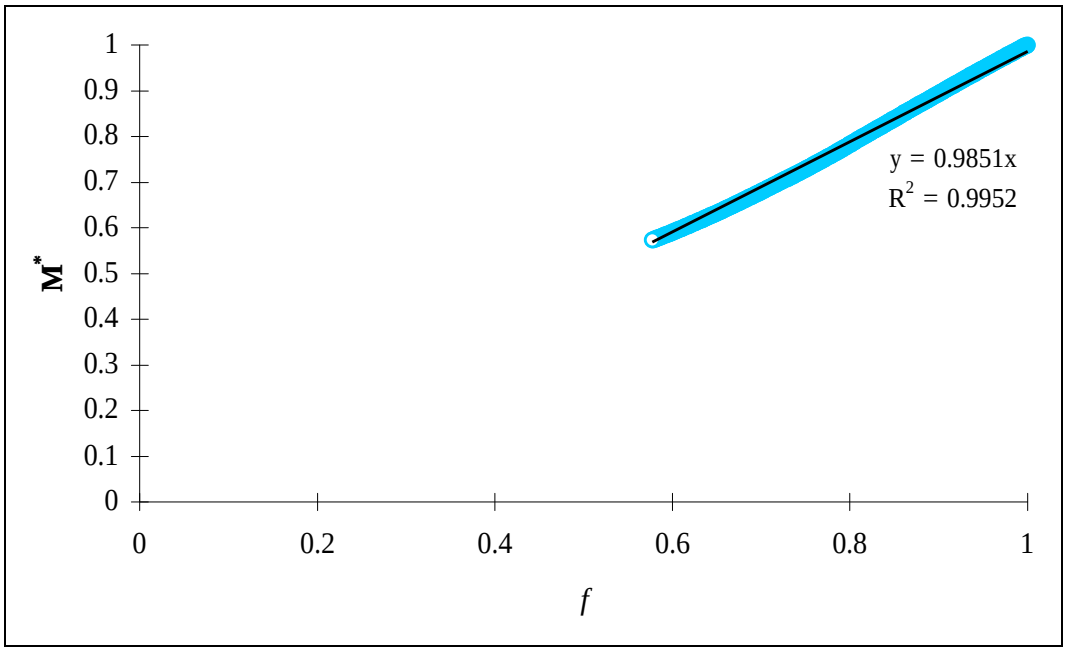

Figure 5-7. NRC-5012 integrated system mass ratio versus integrated flow model dimensionless group.

All of the test data was normalized to the ADS-1 actuation time using the following relations:

$$M' = \frac{M^* - M^*_{ADS-1}}{M^*_0 - M^*_{ADS-1}} \tag{5-9}$$

and

$$f' = \frac{f - f_{ADS-1}}{f_0 - f_{ADS-1}}. \tag{5-10}$$

Using the normalizations, the data can be condensed to a single plot, and the result is shown in Figure 5-8. This result is quite astounding in that it demonstrates that a very simple flow model is capable of accurately predicting the break flow behavior of the APEX test facility to the time of ADS-1 actuation.

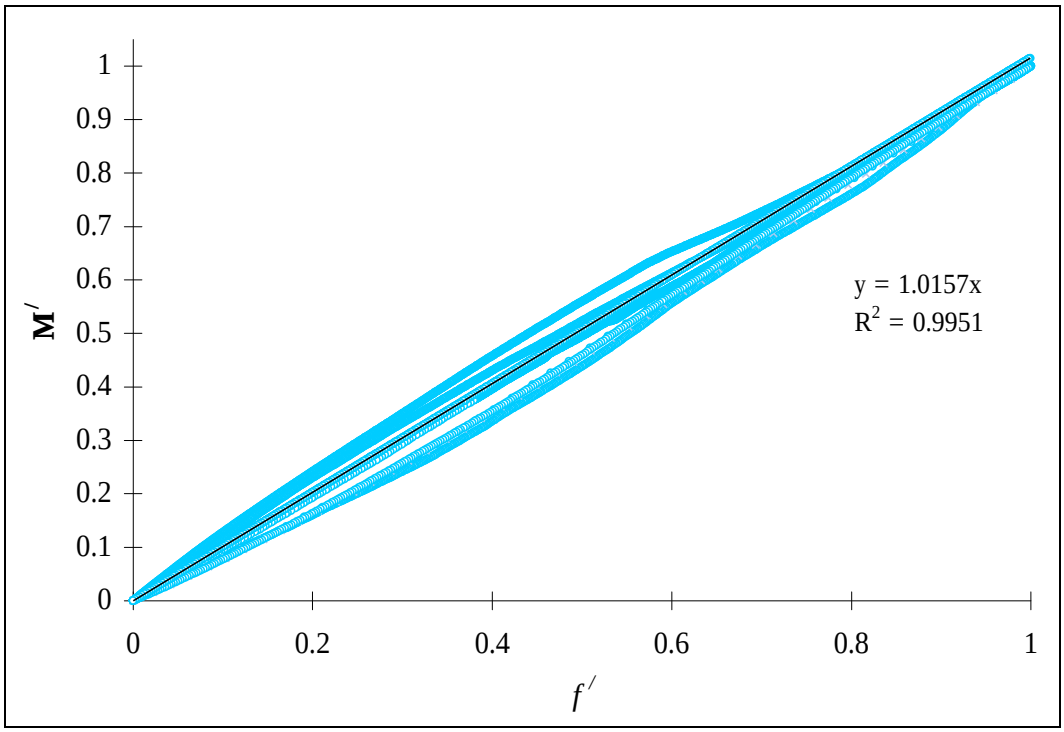

Figure 5-8. Normalized integrated system mass ratio versus normalized saturated flow model dimensionless group for all test data shown in Figure 5-1 through Figure 5-7.

6. Conclusions

This study reviews several aspects of the APEX test facility concerning its capability to accurately simulate the plant conditions of the AP600 – in particular, mass loss quantification through the simulated break geometry and its effects on the primary system depressurization transient.

6.1 Summary

A brief introduction of several critical flow models have been reviewed and some derivations of said model equations have been given. The models discussed included the Homogeneous Equilibrium Model, Equilibrium Rate Model, and Henry-Fauske Subcooled Model. These correlations were then compared to the measured break flow data from the APEX Test facility. It was clearly demonstrated that the equilibrium flow models (i.e., HEM and ERM) were inadequate in predicting the data. This discovery is, of course, a result of the facility's break nozzle geometry having a length-to-diameter ratio (L/D) significantly less than 40, which has been shown to be required to attain equilibrium flow conditions. This inadequacy was also demonstrated by the Relaxation Length Model even though it contains a non-equilibrium parameter. The predictions of the HEM, ERM and RLM under-predicted the data by at least an order-of-magnitude. The Orifice Equation Model over-predicted the initial break flow, but in spite of its simplicity, its predictions were of the same order-of-magnitude as the measured data. To reasonably predict the initial mass flow rate from the simulated break, the Henry-Fauske Subcooled Model should be used with a simple assumption of saturated liquid at a given system pressure. If actual subcooled system conditions are used, the HFSM yields slightly higher flow rates.

The measured break flow data from the APEX Test facility has been demonstrated to be consistent and repeatable. Due to the design of the BAMS, an initial delay exists within the measured flow rates. This delay has been demonstrated to limit accurate measurements of initial break flow rates using a pressurizer liquid level-depression rate for simulated break diameters greater than one inch. This limitation results from the fact that the subcooled blowdown transient occurs much more quickly for the simulated two inch break than for the simulated one inch and one-half inch breaks. However, it is the author's opinion that this delay has little or no negative effect on the BAMS 'ability to accurately measure the flow rates for the entire depressurization transient.

In addition to initial break flow data assessments and comparisons, it was desired to accurately quantify and predict the mass lost from the primary cooling system through the break. To do this, a constant critical mass flux model was defined and compared to the time-dependent integrated mass lost via the break nozzle. The model predicted mass losses based upon initial system conditions, and it was shown to predict the measured data very well. Due to its repeatability, the BAMS data was presented in a non-dimensional form on a single plot, and all of the test data was shown to be reasonably predicted by the model to the time of ADS-1 actuation.

6.2 Recommendations for Future Research

A phenomenon related to the BAMS measurement delay occurs during tests with simulated two-inch and larger break sizes. This phenomenon is a depression in the Break Separator's initial liquid level. Because the liquid level is determined using a *Differential Pressure transducer*, the magnitude of the liquid level depression can not be accurately determined during the initial blowdown. Although the duration of this phenomenon is quite short and its impact on the overall transient is negligible, it is recommended that improved measurement techniques be used for liquid level measurements in the separators.

Bibliography

1. Todreas, N. E. and Mujid S. Kazimi. *Nuclear Systems I: Thermal Hydraulic Fundamentals.* Hemisphere Publishing, Inc., New York, 1990.

2. El-Wakil, M. M. *Nuclear Heat Transport.* International Textbook Company, 1971.

3. Shapiro, A. H. *The Dynamics and Thermodynamics of Compressible Fluid Flow*. The Ronald Press Company, New York, 1953.

4. Fauske, H. K. *Flashing Flows or: Some Practical Guidelines for Emergency Releases.* Plant/Operations Progress, vol. 4 no. 3, pp. 132-134, July, 1985.

5. Henry, R. E. and H. K. Fauske. *The Two-phase Critical Flow at Low Qualities, Part 1 and Part 2.* Nuclear Science and Engineering, vol. 41, no. 1, pp. 79-98, July 1970.

6. Henry, R. E. and H. K. Fauske. *The Two-phase Critical Flow of One-Component Mixtures in Nozzles, Orifices, and Short Tubes.* Journal of Heat Transfer, ASME Transactions, vol. 93, ser. C, no. 2, pp. 179-187, May 1971.

7. Reyes, J. N., Jr. *A Theory of Decompression of Two-phase Fluid Mixtures*. Oregon State University, December 1, 1994. OSU-NE-9407.

8. Wulff, W. *Top-Down Scaling of Reactor Primary System Depressurization by Single-Phase Gas Discharge.* "An Integrated Structure and Scaling Methodology for Severe Accident Technical Issue Resolution, Appendix K". U.S. Nuclear Regulatory Commission, November 1991.

9. Reyes, J. N., Jr., L. E. Hochreiter, A. Y. Lafi, and L. K. Lau. *AP600 Low Pressure Integral Systems Test at Oregon State University Facility Scaling Report.* Westinghouse Report WCAP-14270, January 1995.

10. ASME NQA-1-1989. *Quality Assurance Program Requirements for Nuclear Facilities.* American Society of Mechanical Engineers, United Engineering Center, 345 East 47th Street, New York, NY 10017.

11. Quality Assurance Criteria for Nuclear Power Plants and Fuel Reprocessing Plants. *Appendix B of Title 10, Part 50 of the United States Code of Federal Regulations.* US Government Printing Office, issued annually.

12. LTCT-GAH-001 Revision 2. *AP600 Long Term Cooling Test Project Quality Plan*, Westinghouse Electric Corporation, ESBU Projects Quality Assurance, March 1, 1995.

13. Reyes, J. N., A. Y. Lafi, S. C. Franz and J. T. Groome. Quick-Look Report for OSU APEX NRC-1. 1-*Inch Cold Leg Break with Failure of ADS Valves 1-3.* Department of Nuclear Engineering, Oregon State University, Corvallis, Oregon. July, 1995.

14. Groome, J. T., J. N. Reyes and H. C. Scott. Preliminary Test Acceptance Report for NRC-5005. *Cold Leg #3, ½ -Inch Bottom of Pipe Break with Modified ADS Logic, NRC-5, Revision 0*. APEX Long-Term Cooling Test Facility, Department of Nuclear Engineering, Oregon State University, Corvallis, Oregon. August, 1995.

15. Reyes, J. N., A. Y. Lafi, O. L. Stevens and J. T. Groome. Quick-Look Report for OSU APEX NRC-5105. *½ -Inch Break on Cold Leg #3 with Modified ADS 1-3 Logic and No CMT Refill*. Department of Nuclear Engineering, Oregon State University, Corvallis, Oregon. March, 1996.

16. Groome, J. T., J. N. Reyes and H. C. Scott. Preliminary Test Acceptance Report for NRC-5007. *Cold Leg #3, 1-Inch Bottom of Pipe Break with Modified ADS 1,2 and 3 Logic and No N_2 Injection, NRC-7, Revision 0*. APEX Long-Term Cooling Test Facility, Department of Nuclear Engineering, Oregon State University, Corvallis, Oregon. June, 1995.

17. Reyes, J. N., A. Y. Lafi, O. L. Stevens and J. T. Groome. Quick-Look Report for OSU APEX NRC-7. *1-Inch Cold Leg Break with Modified ADS 1-3 Logic and No Nitrogen Injection.* Department of Nuclear Engineering, Oregon State University, Corvallis, Oregon. October, 1995.

18. Reyes, J. N., A. Y. Lafi, S. C. Franz, S. Asghar and J. T. Groome. Quick-Look Report for OSU APEX NRC-10. *1-Inch Break on Cold Leg #3 with Failure of Three ADS 4 Valves and No CMT Refill*. Department of Nuclear Engineering, Oregon State University, Corvallis, Oregon. March, 1996.

19. Reyes, J. N., A. Y. Lafi, D. A. Pimentel and J. T. Groome. Quick-Look Report for OSU APEX NRC-3. *2-Inch Cold Leg Break with Long-Term Cooling and Check Valve CSS-912 Removed*. Department of Nuclear Engineering, Oregon State University, Corvallis, Oregon. March, 1995.

20. Reyes, J. N., A. Y. Lafi, S. C. Franz and J. T. Groome. Quick-Look Report for OSU APEX NRC-11. *2-Inch Cold Leg Break with Modified ADS 1-3 Logic and No CMT Refill*. Department of Nuclear Engineering, Oregon State University, Corvallis, Oregon. August, 1995.

21. Reyes, J. N., A. Y. Lafi, D. A. Pimentel and J. T. Groome. Quick-Look Report for OSU APEX NRC-12. *Two-Inch Break on Cold Leg #4 with Modified ADS 1-3 Logic and No CMT Refill*. Department of Nuclear Engineering, Oregon State University, Corvallis, Oregon. December, 1995.

22. Yundt, M. *OSU APEX Instrument Calibration Database*. Department of Nuclear Engineering, Oregon State University, Corvallis, Oregon. Updated April 10, 1996.

Index

O

P

Q

R

S

T

V

W